DØNote 5059
Version 2.4

DØ Search for Stopped Gluinos using p14 Data

Andrew Haas [1]

1. Columbia University / Nevis Labs – USA

February 8, 2007

Abstract

A long-lived gluino is a generic prediction of several models of beyond the Standard Model physics, such as Split-SUSY. Some fraction of the hadronized gluinos (R-hadrons) can lose enough momentum to come to rest in the calorimeters. About 410 pb^{-1} of Run II data reconstructed with p14 software is analyzed in search of stopped gluinos decaying into a jet and a neutralino. No excess is observed above the expected background from cosmic-muon induced showers, and limits are placed on the stopped gluino cross-section x BR(G$\rightarrow g\chi_1^0$) as a function of the gluino and neutralino masses, for gluino lifetimes between $30\mu s$ - 100 hours.

1 Introduction and Theory

Split-Supersymmetry is a relatively new variant of Supersymmetry, in which the Supersymmetric scalars are heavy (possibly GUT-scale) compared to the (SUSY) fermions [1]. This simple relaxation of one of the foundations of standard Supersymmetry avoids many fine-tunings which must be incorporated to remain consistent with observations while still preserving the favored consequences. A dark-matter candidate is still present in the theory to explain the observed cold-dark matter density in the Universe, GUT-scale coupling unification still occurs, and the required Supersymmetry is still present as needed for String theory. Due to the scalars' high masses, the gluino decays (into squarks and the neutralino LSP) are suppressed, and the gluino lifetime is determined by this SUSY-scalar mass scale (M_{SUSY}). The gluinos have time to hadronize into "R-hadrons" [1], colorless bound states of a gluino and other quarks or gluons.

At the Tevatron, R-hadrons could be pair produced through strong interactions. If $M_{SUSY} > 10^6 GeV$, which is likely, since the natural M_{SUSY} is the GUT scale, the R-hadrons live long enough ($> 10ns$) to reach the DØ calorimeters. Hadronization models of gluinos [2] predict a spectrum with degenerate light meson-like states, leading to a fraction of R-hadrons which are electrically charged of about 1/2. R-hadrons can also become charged when passing through matter. As studied in [3], some charged R-hadrons can become "stopped gluinos", by losing all of their momentum through ionization and coming to rest in the calorimeters. Most of these stopped gluinos would later decay into a jet (from a gluon) and a neutralino (LSP).

This analysis searches for stopped gluinos (G) produced at the Tevatron in Run II, decaying into a jet plus neutralino. The stopped gluino lifetime is assumed to be long enough such that the decay of the gluino occurs during a bunch-crossing adequately later than the one which produced it (about $30\mu s$). If the decay were to occur sooner than this, it is possible that the trigger could be dead during the bunch-crossing containing the decay. Some parts of the detector could still be being read-out from the event which produced the gluino-pair. The decay is also assumed to take place soon enough such that data is consistently being recorded during the decay. The efficiency for recording the gluino decay is modeled as a function of the gluino lifetime, up to a lifetime of 100 hours [2]. Since the decay most likely occurs during a bunch-crossing with very little other high-p_T activity, the signal signature is a largely empty event with a single high-p_T jet and thus large missing E_T.

It is worth noting that several other interesting and more complicated related signatures are also available. When one of the pair-produced gluinos stops in the calorimeters, 30% of the time the other one stops as well [3], since the p_T of the two gluinos are highly correlated in each event. This makes possible the search for "double-bang" events, where two decays are observed close in time. These could be a way to directly measure the gluino lifetime and thus M_{SUSY}. Another phenomenon is the two-jet decay plus MET, coming from the decay $G \rightarrow q\overline{q}\chi_1^0$, which may be possible to distinguish

[1] They are called "R-hadrons" because they are only long-lived if R-parity is conserved, in which SUSY particles have opposite R-parity from Standard Model particles.

[2] In many models, and particularly for gluinos >500 GeV, Big-Bang nucleosynthesis constrains the gluino lifetime to be <100 seconds, but lighter gluinos could live up to 100,000 years.

from the single-jet decay. The branching fraction of double- to single- jet decays would also provide information on M_{SUSY}. Finally, it may be possible to observe the decay $G \to \chi_2^0 j \to \chi_1^0 \mu^+ \mu^- j$ with two muons coming from the jet location with an invariant mass less than or equal to the mass difference of the two neutralinos. However, the search for and study of these processes will be left to future investigations.

2 Simulation

The stopped gluino decays a majority of the time into a gluon plus a neutralino (LSP). There is also some branching fraction to $q\overline{q}$ plus a neutralino, possibly up to 50% depending on various model parameters, but these decays will be ignored. The analysis specifically searches for mono-jet events, and limits will be set on the cross-section x BR to a gluon + LSP only. The radial location of the gluino when it decays depends on the way the gluinos lose energy via ionization and stop in the calorimeters. This calculation was performed [3] for a distribution of material similar to the DØ calorimeters (production at the Tevatron), as shown in Figure 1. The $|\eta|$ distribution of the stopped gluinos is determined by the fact that gluinos would tend to be produced near threshold at the Tevatron, and that only slow gluinos would stop. Therefore the gluinos are expected to be distributed proportional to $\sin\theta$, and more than 75% of gluinos which stop are in $|\eta|<1$. This can be understood as being due to the fact that gluinos produced centrally will have smaller total momenta, since p_z is small. The gluinos are randomly oriented in space when they decay, thus the gluon is emitted in a random direction. The energy of the gluon (jet) depends on the gluino and LSP masses:

$$E = (M_g^2 - M_{LSP}^2)/2M_g \tag{1}$$

To simulate the jets that would be produced by stopped gluino decays, Pythia was used to produce Z+gluon events (MSEL=13) with the Z forced to decay to neutrinos. The location of the interaction point (the gluino decay location) was set to (x,y,z)=(0±20,120±120, 0±80) cm, near the outside of the EM calorimeter layers, by overwriting the mcvertex.rcp file. The vertex is chosen in each event according to a Gaussian distribution in each coordinate. The 80 cm RMS of the z vertex location roughly corresponds to the $|\eta|$ distribution of the stopped gluinos, but events are further weighted such that the final events are proportional to $\tanh\eta = \cos\theta$, as expected for stopped gluinos. Events are also weighted such that the radial distribution corresponds to that expected for stopped gluinos as shown in Figure 1, assuming a 3mb charge-conversion cross-section. The other values for the charge-conversion cross-section are used to estimate the systematic uncertainty on the stopped-gluino detection efficiency caused by the change in the radial profile (see Section 10). Initial-state radiation (ISR) was switched off in Pythia, and so were multiple parton interactions, since we do not really want to simulate a full $p\overline{p}$ beam. The $|\eta|$ of the gluon was restricted to be less than 0.1 at the generator level and a p_T cut was applied at the generator level corresponding to Equation 1, which prevents the gluon jet from obtaining extra energy from the boost of the system along the beam direction. The spectator particles coming from the rest of the $p\overline{p}$ interaction, such as the underlying event, were removed

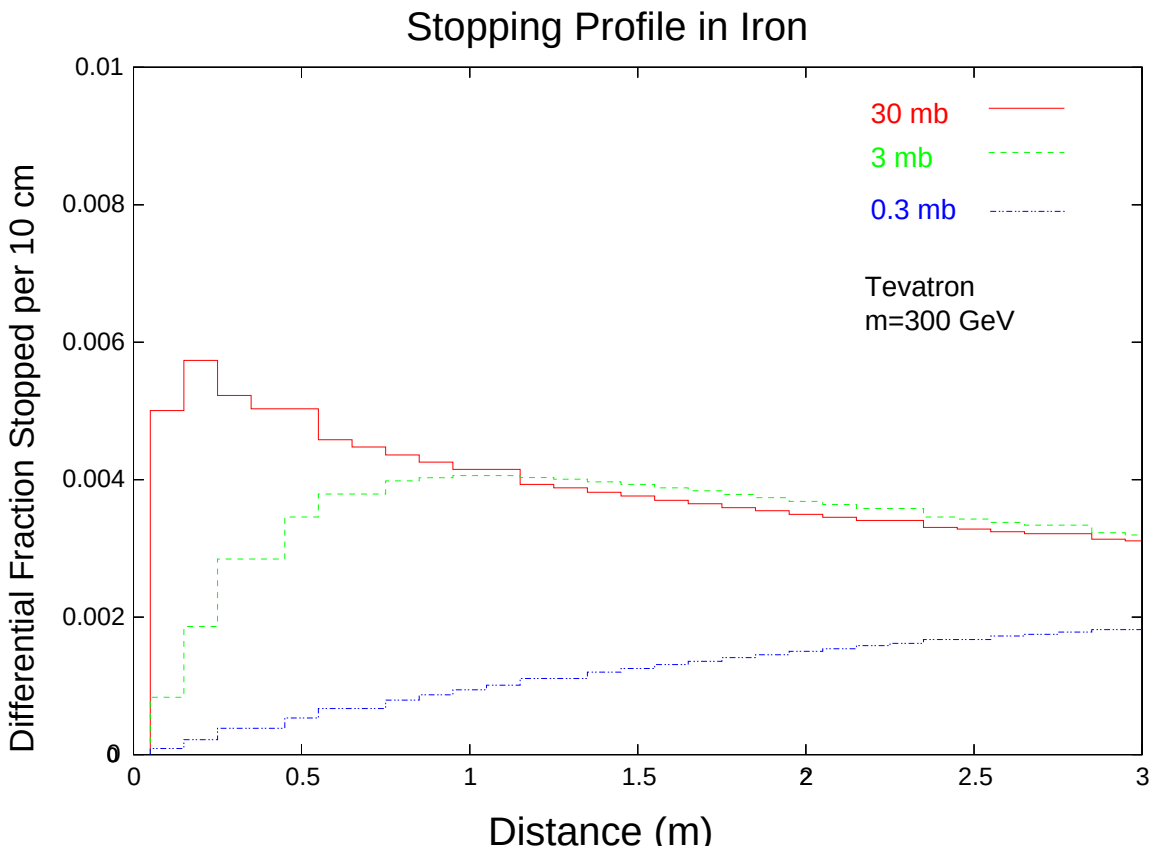

Figure 1: The radial distribution of the stopped gluinos, as calculated in [3]. The three histograms are for various assumptions of the cross-section for converting a neutral R-hadron to a charged one upon passing through matter. The average of the 3 conversion cross-sections is used, and the extreme values are used to estimate the systematic uncertainty on the stopped-gluino detection efficiency caused by the change in the radial profile.

at the generator stage by stopping (setting momenta to 0.01 GeV) all particles with $|pz/E| > 0.95$. Finally, a random 3D rotation was applied to the remaining particles, to simulate the random decay axis of the gluino.

Four samples of "stopped gluino MC" were privately produced using release p14.07.00 (and p14.06.01 for DØReco), containing 1000 events each, and were fixed with TMB-fixer in release p14.fixtmb2.03. The samples had mass cuts at the generator level [3], of 195-205, 295-305, 395-405, and 495-505 GeV, corresponding to gluino masses of about 200, 300, 400, and 500 GeV, respectively, for an LSP mass of 90 GeV (the Z behaves similarly to an LSP of the same mass). Using Equation 1, we note that these samples thus correspond to generated parton (jet) energies of 80, 137, 190, and 242 GeV, respectively. A little more than half the gluino energy goes to the LSP. Plots of the simulated gluino jets are shown in Figure 2, for jet energy, n90 (number of towers needed to make up 90% of the jet E_T), number of jets (with E_T>8 GeV), η, ϕ-width (the E_T-weighted RMS of the jet towers' ϕ), and η-width (the E_T-weighted RMS of the jet towers' η). Some event displays of simulated events made with the d0ve program are shown in Figures 3 - 7.

3 Data Sample

Data taken from November 2002 – August 2004, were reconstructed and corrected with the p14.03.01 – p14.06.01 versions of the reconstruction software, and corrected with "PASS2" software. Since no $p\overline{p}$ beam-interaction is expected to be correlated with the stopped gluino decay, the "DIFF" skim was selected and one of the "GAPSN" triggers was required for each event. Of course, minimum-bias interactions can occur during the same bunch crossing as the decay, and efficiency corrections will be made for this. The "QCD" skim with the JT125_TT trigger required was used for studying the efficiency of the GAPSN trigger requirement as well as the total integrated luminosity of the sample. The integrated luminosity of the JT125_TT trigger for this data sample was calculated to be 410 pb^{-1}, after data quality cuts (see Section 5).

The GAPSN triggers require no firing of either the North or South luminosity counters, placed on the front face of the end-cap calorimeters at high $|\eta|$. Two versions exist, the first (JT_15TT_GAPSN) has lower calorimeter thresholds and is prescaled at some very high luminosities, and the second (JT_45TT_GAPSN) is always un-prescaled. The first trigger requires 2 L1 calorimeter towers above 3 GeV and a 15 GeV L3 jet. The second requires 2 L1 calorimeter towers above 5 GeV and a 45 GeV L3 jet. Each event is required to have fired one of these two triggers. About 7.9 million events exist in the initial trigger-selected, skimmed, data sample. This corresponds to a data rate of about 0.5 Hz.

[3] CKIN(1)-(2) in Pythia

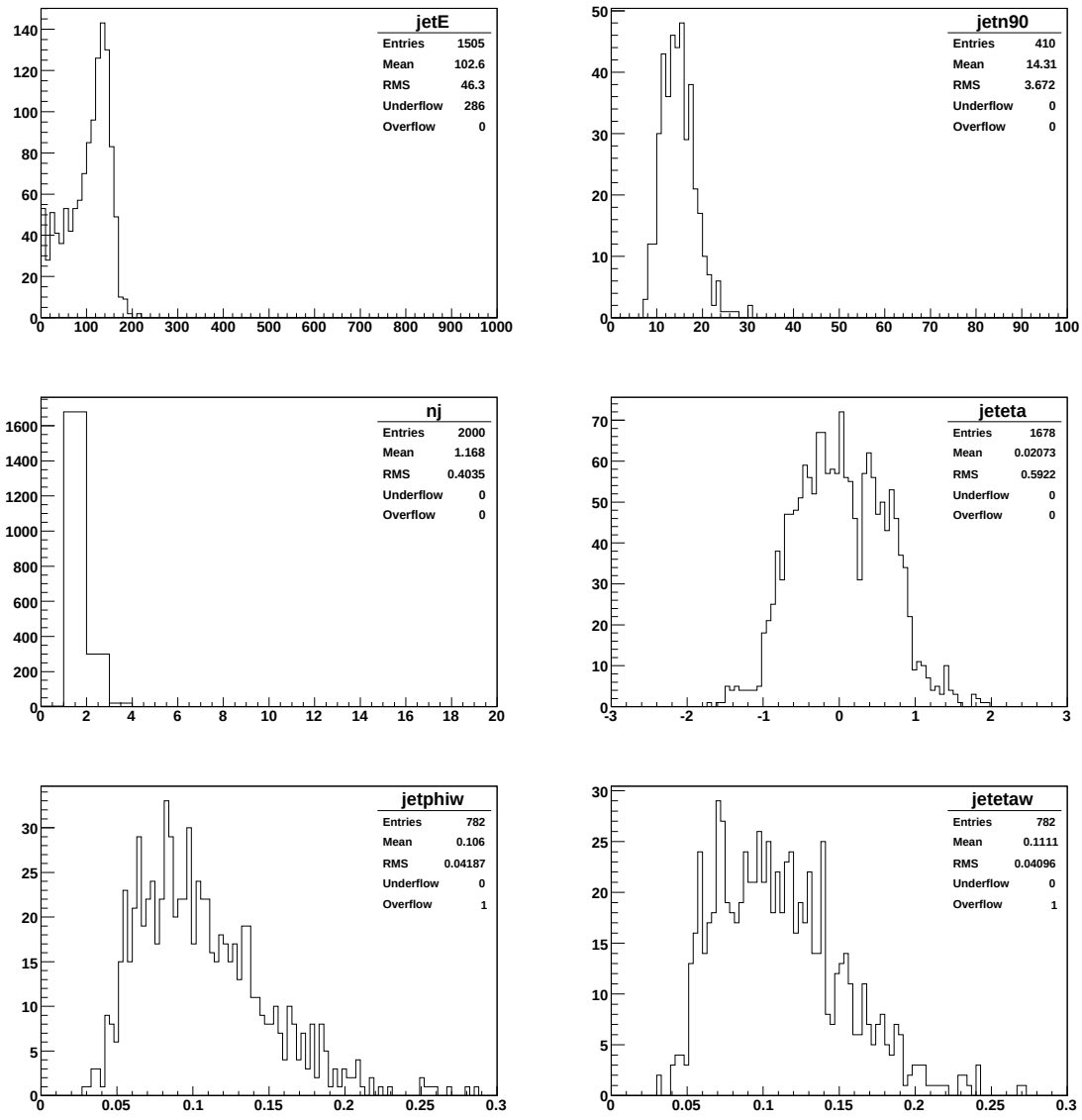

Figure 2: The jet properties for the m_G=400 GeV simulated MC sample.

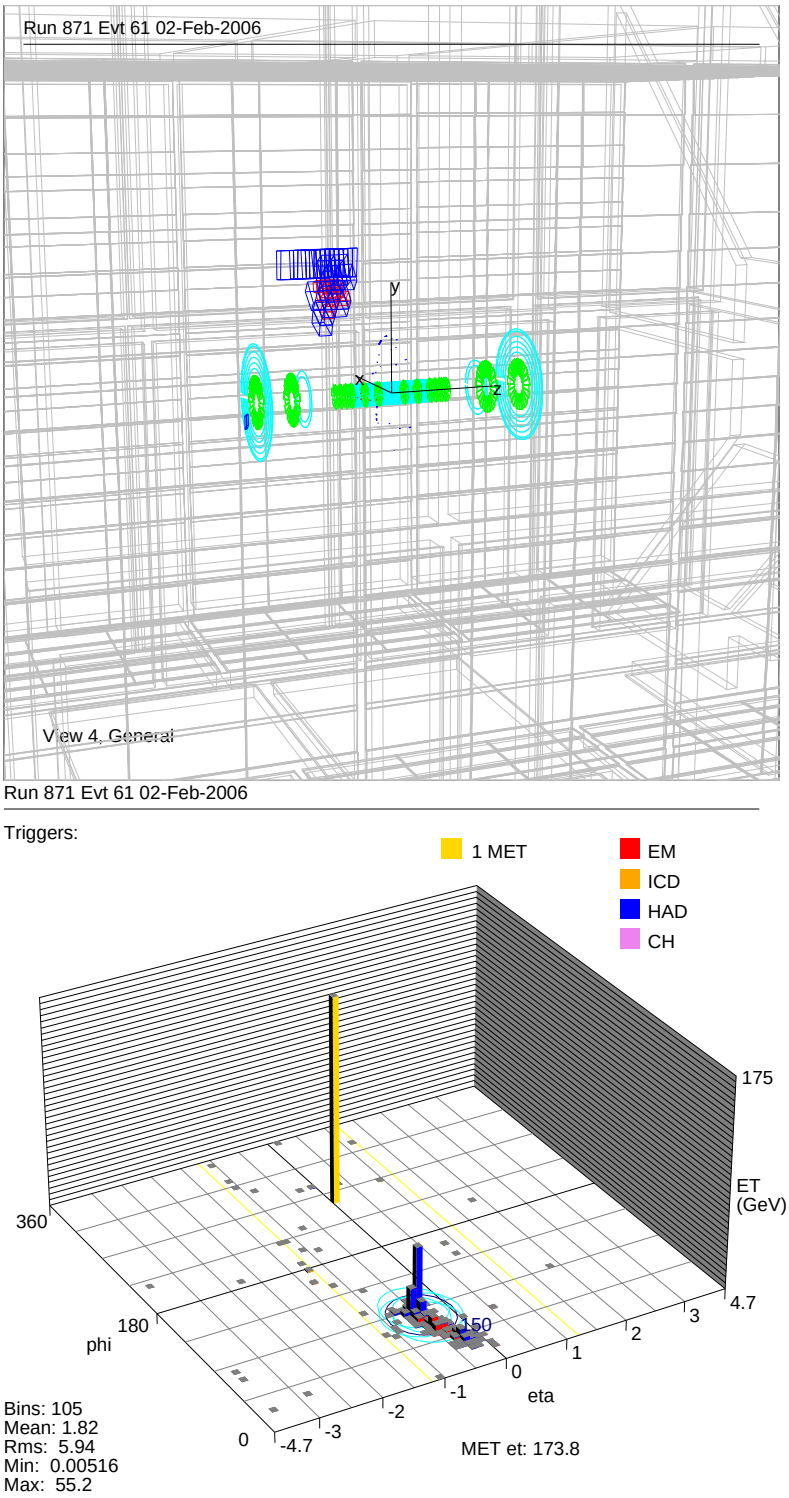

Figure 3: A fairly typical m_G=400 GeV simulated MC event.

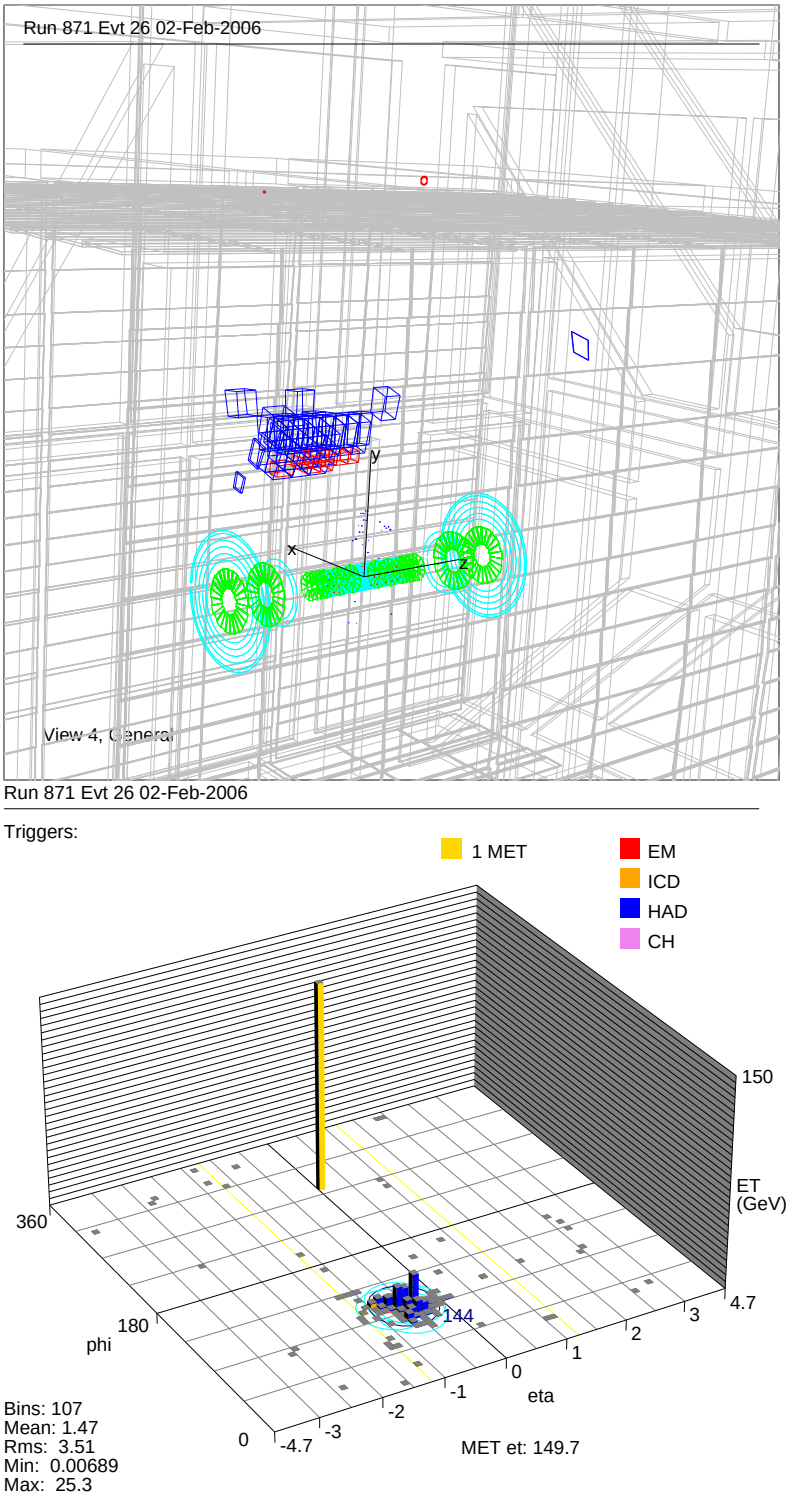

Figure 4: A m_G=400 GeV simulated MC event where the jet was generated nearly parallel to the beam.

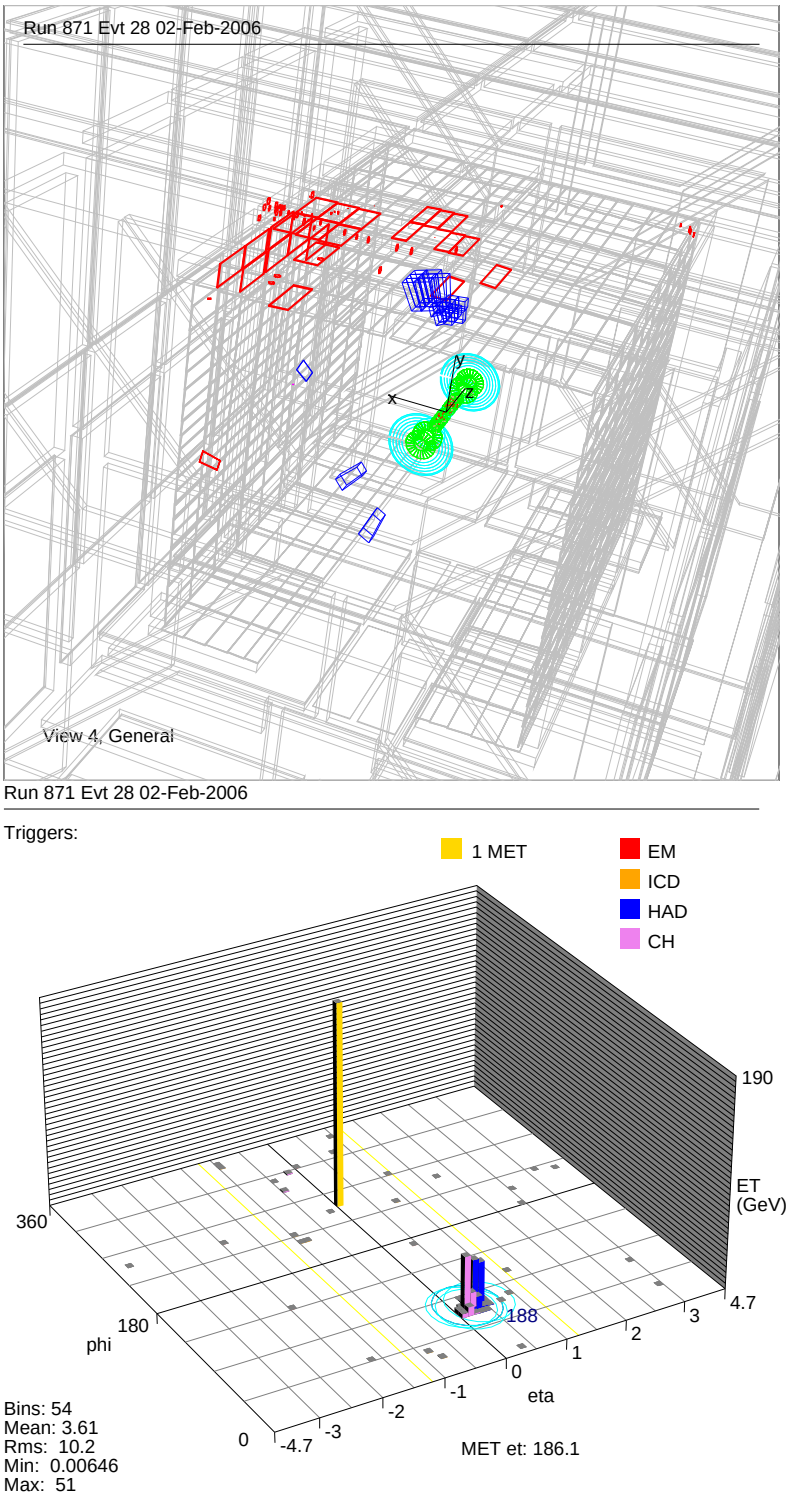

Figure 5: A m_G=400 GeV simulated MC event with a large "A-layer muon splash".

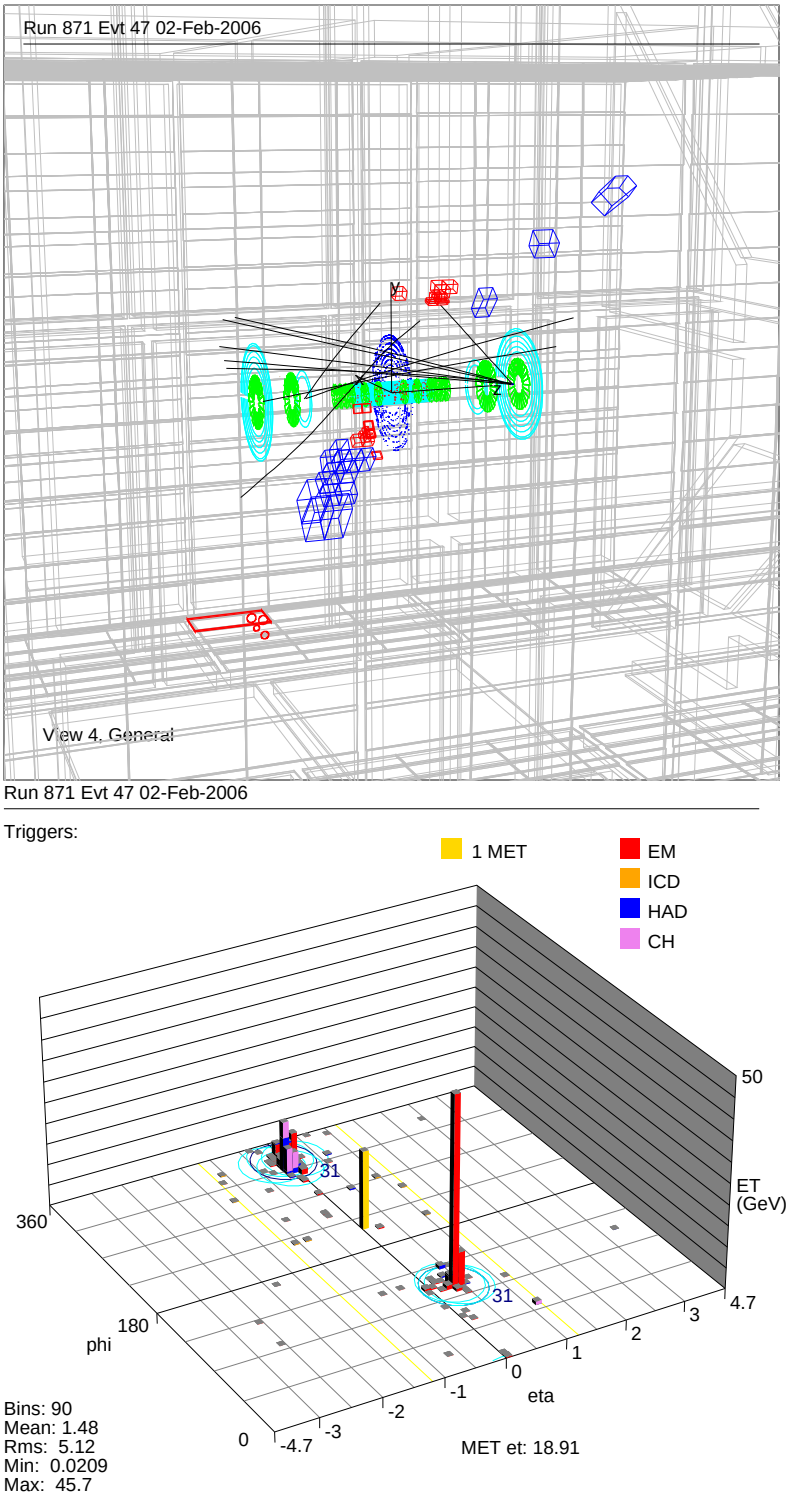

Figure 6: A m_G=400 GeV simulated MC event where some of the shower has gone back across the tracking chamber to the other side of the calorimeter.

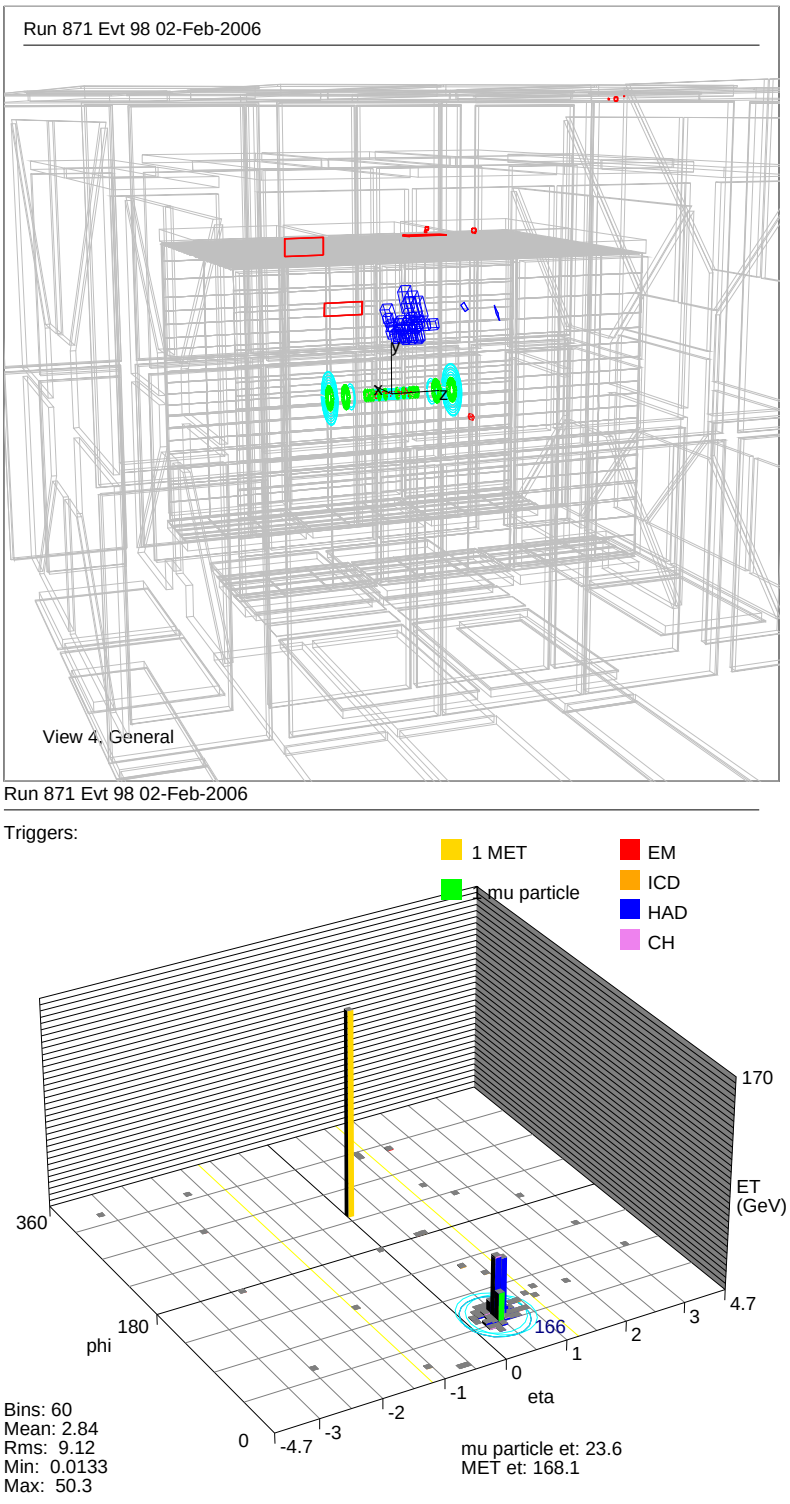

Figure 7: A m_G=400 GeV simulated MC event that has a reconstructed muon from a particle (possibly a muon) punching through the toroid.

4 Object Identification

Jets were reconstructed with the Run II Improved Legacy Cone Algorithm (ILCA) [4] with cone size of 0.5 (JCCB). The T42 hot-cell killing algorithm was used during reconstruction, as for all of PASS2. Jets were not required to pass any additional quality criteria and their energies were not corrected back to the particle level for detector and physics effects using any jet energy scale factors, since the assumptions used to derive these corrections (a projective geometry, etc.) are no longer valid for these jets. However, the relative data/MC JES correction was applied to MC jets, in order to compare the uncorrected jet energies between data and MC and estimate the systematic uncertainty in the jet energy scale. In addition, jet energies in the simulation were corrected (downwards) according to a model of the out-of-time calorimeter response (see Section 9).

Muons were reconstructed and no extra quality criteria or corrections were applied. They were separated by their number of "segments" (NSEG) as 1, 2, or 3. Muons with NSEG=1 are A-layer only muon segments, whereas the other muons also have matching segments in the B/C layers, outside the iron toroid. No inner-track match was required for the muons, and no timing cuts were applied.

5 Pre-selection

In addition to the trigger criteria described above, loose cuts were used to select a initial data sample to study.

- Require "good" muon and SMT and CFT runs, for rejection of cosmic and diffractive events.
- Require exactly one JCCB jet in the event. This helps to reduce certain kinds of detector noise, and also simplifies the analysis.
- Jet E >90 GeV. This avoids noise jets and is also high enough such that the calorimeter part of the trigger is nearly 100% efficient.

6 Sources of Background

We now look at the data to understand the sources of backgrounds that contribute. We will need to understand the backgrounds carefully, in order to be able to devise cuts against them while remaining efficient for signal, as well as being able to estimate the amount of (and energy spectrum of) remaining background as accurately as possible.

The major source of background is cosmic muons. They are able to fake a gluino signal because they can initiate a high-energy shower within the calorimeter. The rate for a cosmic muon to deposit enough energy to pass the basic pre-selection criteria (E>90GeV) is observed to be quite large, about 0.1 Hz. Hard Bremsstrahlung emission is responsible for the majority of the showers. (The probability for a hard-photon of at least 10% of the muon energy to be created in 3m of Iron is about 0.1%.) Fortunately,

these showers tend to be very narrow, since they are electro-magnetic in nature and thus have small interaction lengths compared to hadronic showers. Most of the energy is deposited in a few calorimeter cells, see Figure 8. However, sometimes a wide, hadronic-like, shower can be created either due to real deep-inelastic scattering, fluctuations of the shower, or detector effects, as seen Figure 9. Cosmic muons can also mimic other, rarer, signal-like qualities, such as the large muon A-layer "splash", as seen in Figure 10.

Of course, cosmic muons can usually be identified by the presence of a high-energy muon, either entering or exiting the detector, using the muon detectors. In particular, a coincidence of muon hits in the outer two (B,C) layers of the muon system are very strong evidence of a muon. The A-layer hits are often also caused by the signal, due to particles escaping the calorimeters, so these hits are difficult to use for background rejection. (These particles are nearly all absorbed in the Iron toroid magnets before reaching the B,C layers, so do not cause signals often in these outer layers.) In fact, the A-layer hits are used if they are consistent with the geometry of a muon passing through the detector (back-to-back) and not near a hadronic shower. (See Section 7 for complete description of these criteria.) However, sometimes no muon is detected, due to detector inefficiencies or the limited detector acceptance up to $|\eta|<2$. Muons can also be detected, in principle, through their ionizing interactions in the calorimeter, where they are minimum-ionizing particles (MIP's). However, these MIP trails are difficult to identify in this geometry where the direction of the muon path is unknown, and also there is a large shower nearby which overlaps with the energy deposited by the MIP. (These MIP tracks are easier to identify for muons on a well-defined path, such as muons traveling outward from $p\overline{p}$ collisions, and when they are not near a jet shower.)

Another source of background events is beam-halo muons, or "beam-muons". These are muons, in-time with the bunches of $p\overline{p}$, and traveling nearly parallel to the beam, as seen in Figure 11. Often, a muon scintillator hit or two can be associated with the muon, and the muon can be seen to be in-time, with $\Delta t<10$ns [4]. Another feature of the beam-muons is that they are nearly all in the plane of the accelerator beam, i.e. with ϕ very near to integer multiples of π, as seen in Figure 12. This may be due to the geometry of accelerator magnets or collimators, or gaps in the shielding at either DØ or CDF. Beam-muon showers are also typically very narrow in ϕ-width, even narrower than cosmic muon showers. Since beam-muons are traveling parallel to the beam, the ϕ-width is small no matter how long the shower extends along the path of the muon. For the same reason, the η-width of beam-muons tends to be larger than for cosmic muons. Comparisons of these quantities for beam-muons and cosmic-muons can be seen in Figure 13.

Since we are using the GAPSN triggers, nearly all of the $p\overline{p}$ beam produced backgrounds are eliminated. An exception is double diffractive events with large momentum transfer. Figure 14 shows an example of such an event. However, after requiring *no PV* to be reconstructed and large $\not\!\!E_T$ (implicit from the choice of only one central jet with

[4] Δt for muon hit is (time hit occurred) - (time a hit would occur from a muon coming from the beamline in this bunch crossing). So, it's the extent to which the hit is early or late, compared to a hit from a "standard muon", traveling at speed c from the beamline.

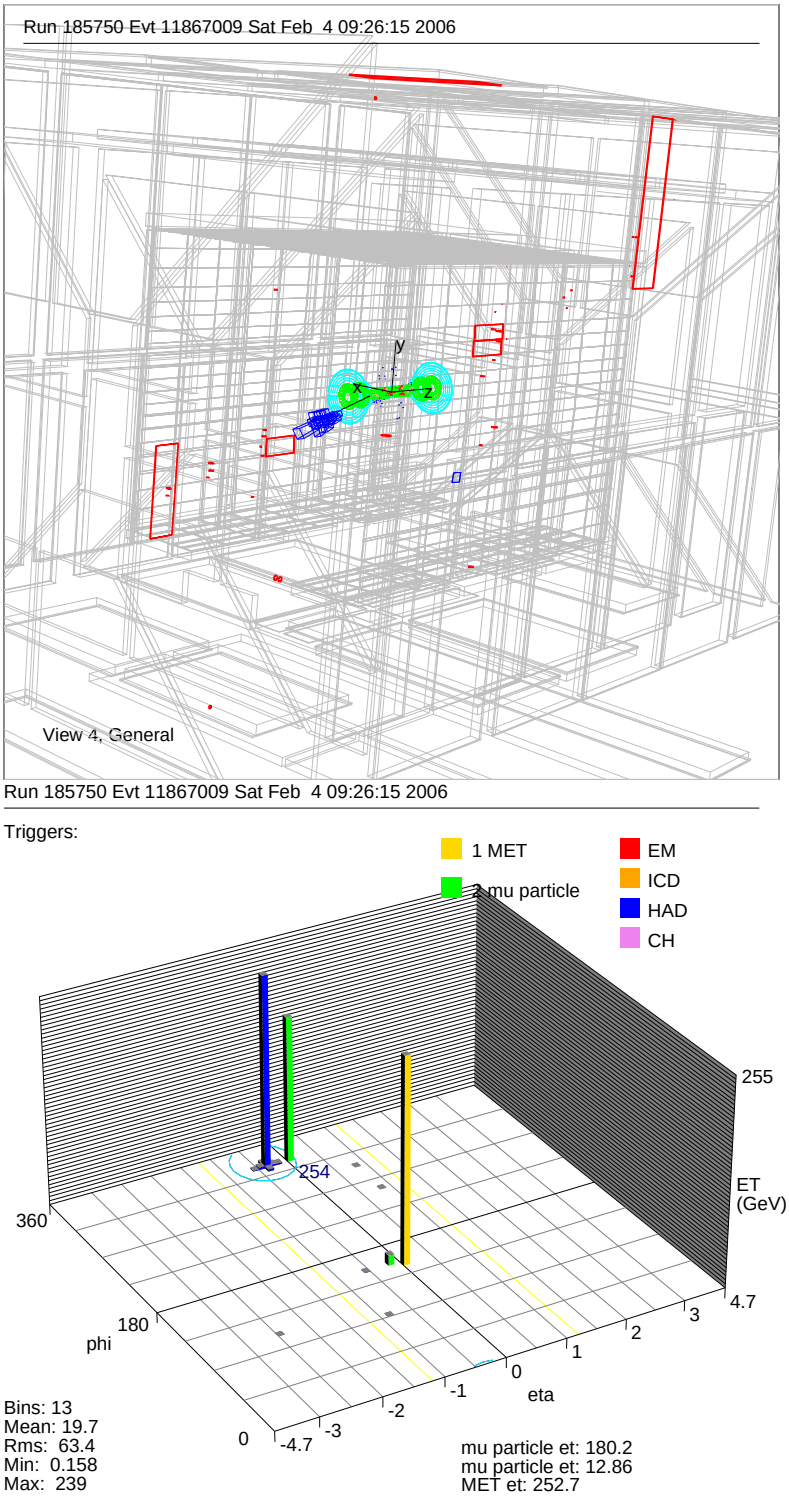

Figure 8: A typical cosmic muon, hard Bremsstrahlung, shower. There are reconstructed muons and a very narrow energy deposit.

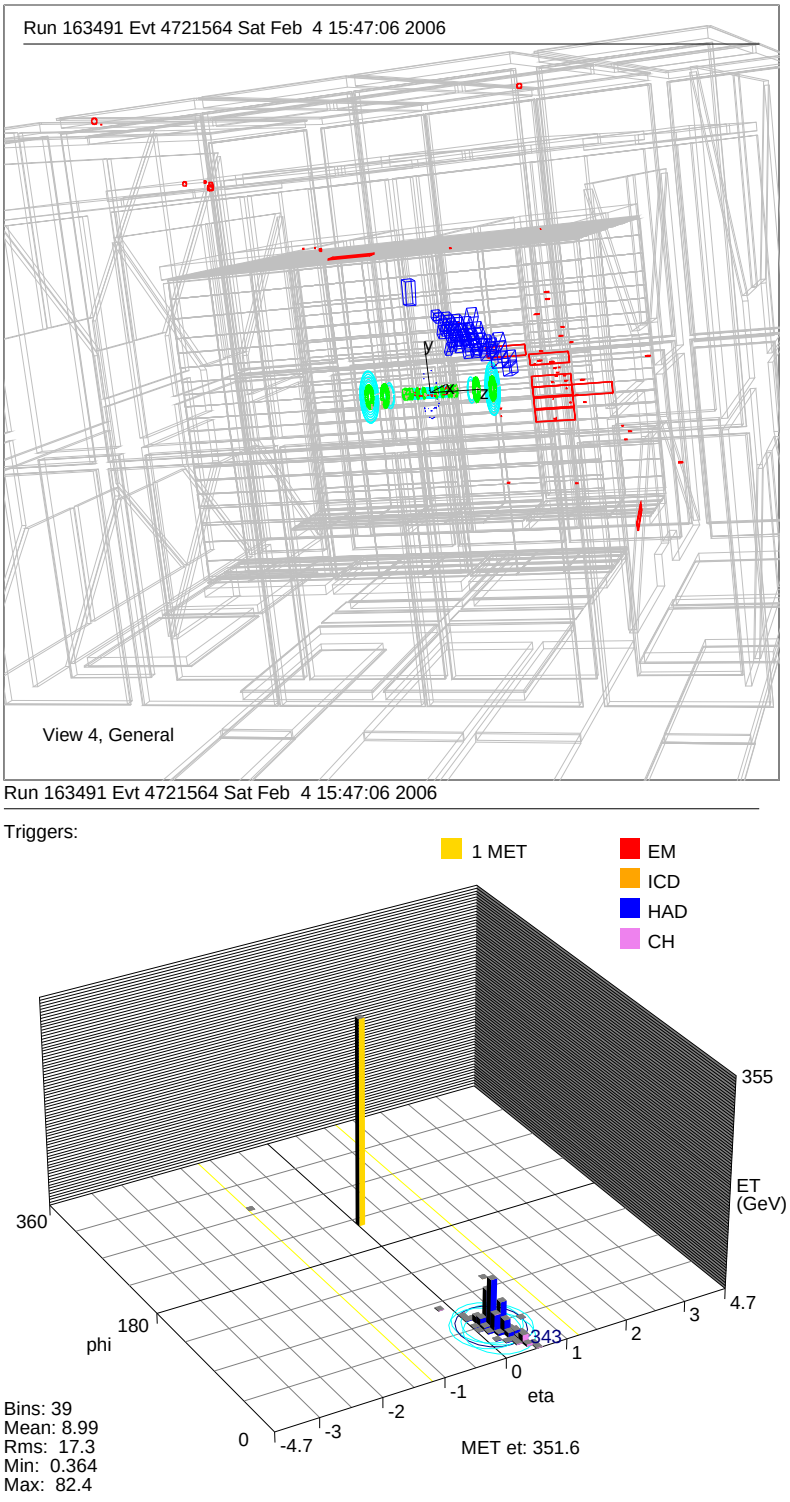

Figure 9: A wide, hadronic-like, cosmic muon shower. This event also contains an A-layer "splash".

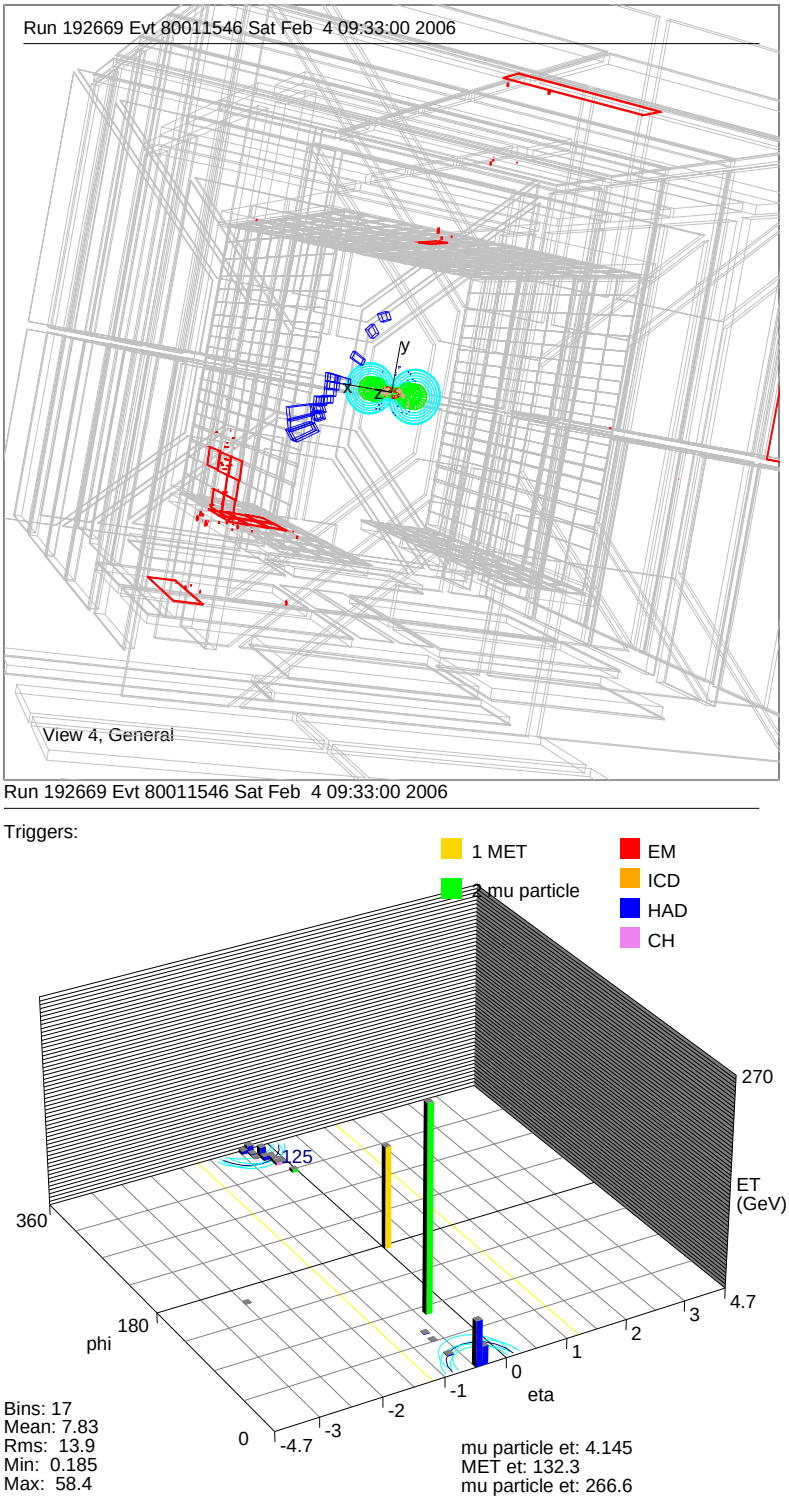

Figure 10: A cosmic muon shower with a large A-layer muon "splash".

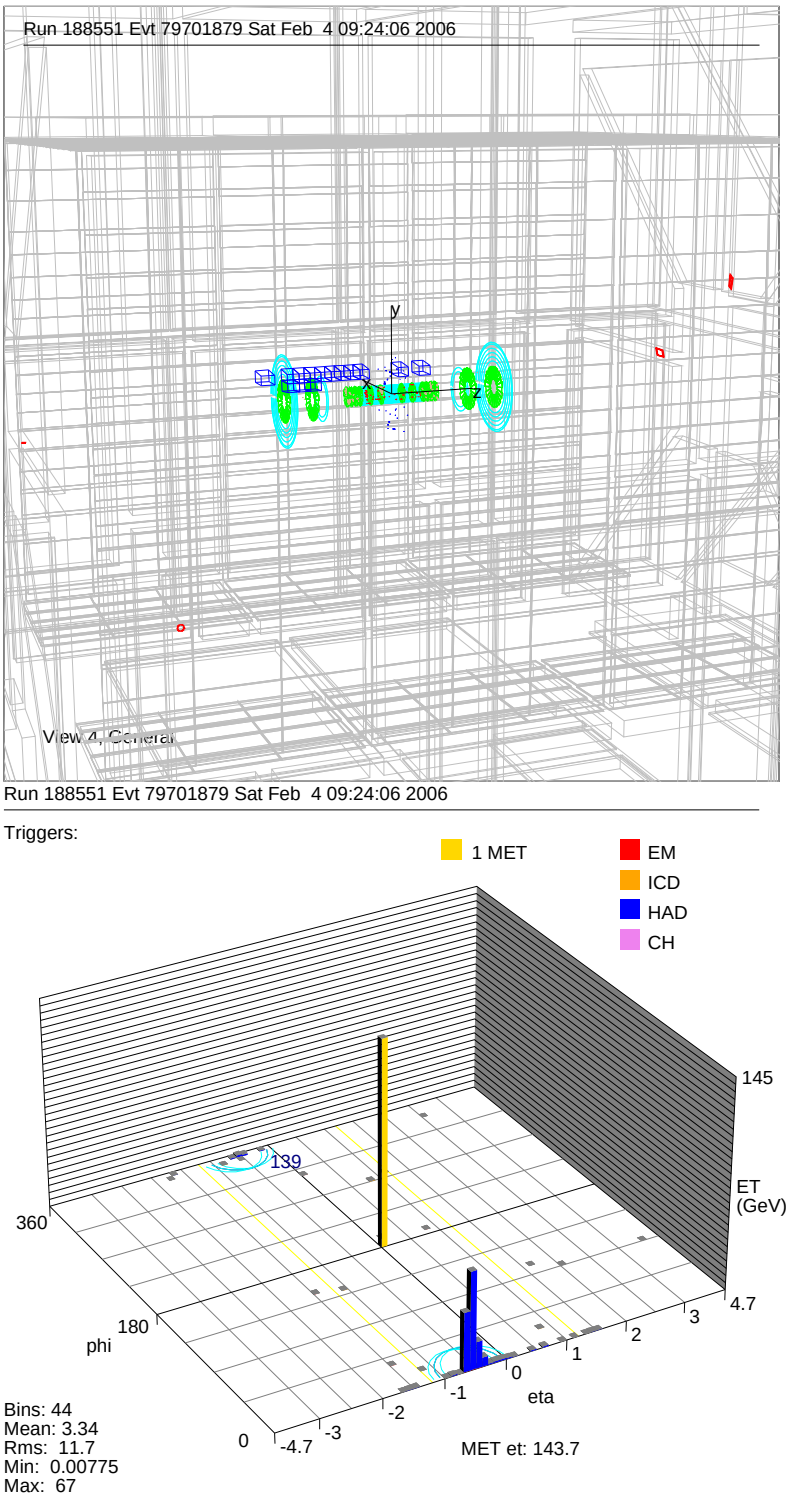

Figure 11: A typical beam-muon shower. The jet is very narrow in ϕ, but long in η, and centered at an integer multiple of π (in the plane of the accelerator).

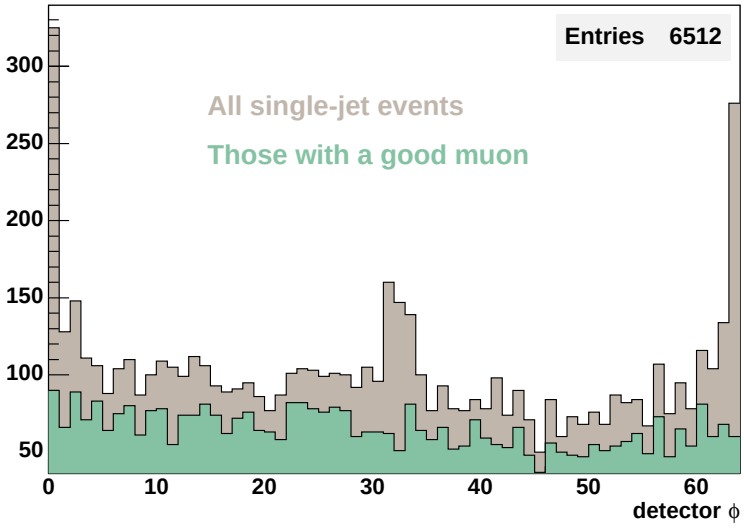

Figure 12: The ϕ of jet showers from all sources, beam-muons and cosmic-muons (grey), and good cosmic muons (green). The beam-muon showers are highly localized near integer values of π, in the plane of the beam.

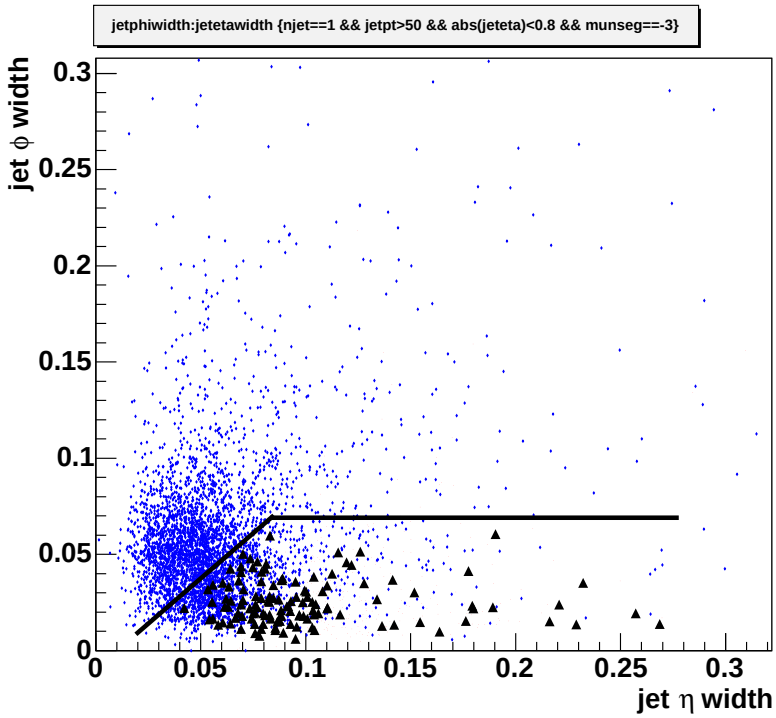

Figure 13: The ϕ vs. η of jet showers from beam-muons (black triangles) and cosmic-muons (blue dots). The beam-muon showers are selected by requiring an associate "in-time" muon scintillator hit. The beam-muons are narrower in ϕ-width but wider in η-width than the cosmic showers, due to the fact that they are parallel to the beam.

E>90 GeV), these events are eliminated. Events in the same data sample were studied where the requirement of exactly one jet was relaxed to understand the $\not\!\!E_T$ spectrum and PV reconstruction efficiency for beam-related backgrounds. Figure 15 shows the $\not\!\!E_T$ distribution for this more inclusive data-set. Two things are clear from this distribution: very few diffractive events are expected to have large $\not\!\!E_T$ (>50GeV) and the efficiency for reconstructing the PV for diffractive events is high (>95%). Thus, <0.1 diffractive events are expected to pass the requirement of exactly one (central) jet with E>90GeV and no reconstructed PV, making this a negligible background.

Other small sources of background considered are cosmic neutrons and neutrinos. Neutrons would be more effective in creating wide hadronic showers, but their rate is about 1/1000th that of cosmic muons of similar energy, and they also would be unlikely to penetrate the Iron toroid magnets. In the event that one did reach the calorimeter, they would most likely shower in the outer coarse-hadronic layer, which is not part of the L1 calorimeter trigger. Thus, we expect that the number of cosmic neutron events in the data sample is very low. Neutrinos are copious, but have a very low interaction rate. A back-of-the-envelope calculation predicts a neutrino-shower rate of about 0.1/year.

Finally, since we are looking for a very rare process, occasional detector malfunctions could also fake a signal. However, these problems tend to be isolated to a specific set of runs, a specific detector region, or both. See Figures 16 and 17 for displays of the most frequent problems. Also, the detector problems would have to be correlated between the calorimeter and muon systems in order to pose a significant background in this analysis while not being detected in other control samples.

7 Event Selection

Now that the background sources are understood and the gluino signal is simulated, we can make selections to reduce the backgrounds while still remaining efficient for the gluino signal.

- Jet $|\eta|$<0.9. The ICR and forward regions of the calorimeter were observed to have some difficult detector problems (hot spots). Also, the gluino signal tends to be concentrated in the central regions.

- No reconstructed primary vertex. This usually means that no tracks were reconstructed, although sometimes a track was found but does not come close to the beam axis. This requirement removes background from diffractive events very effectively.

- The rectangular region ($-.55 < \eta < -.75$, $1.3 < \phi < 1.5$) was too noisy and therefore all events in that region were rejected. (See Figure 17 above.)

- Jet E <900 GeV. This avoids certain kinds of detector problems and is besides un-physical for a gluino at the Tevatron.

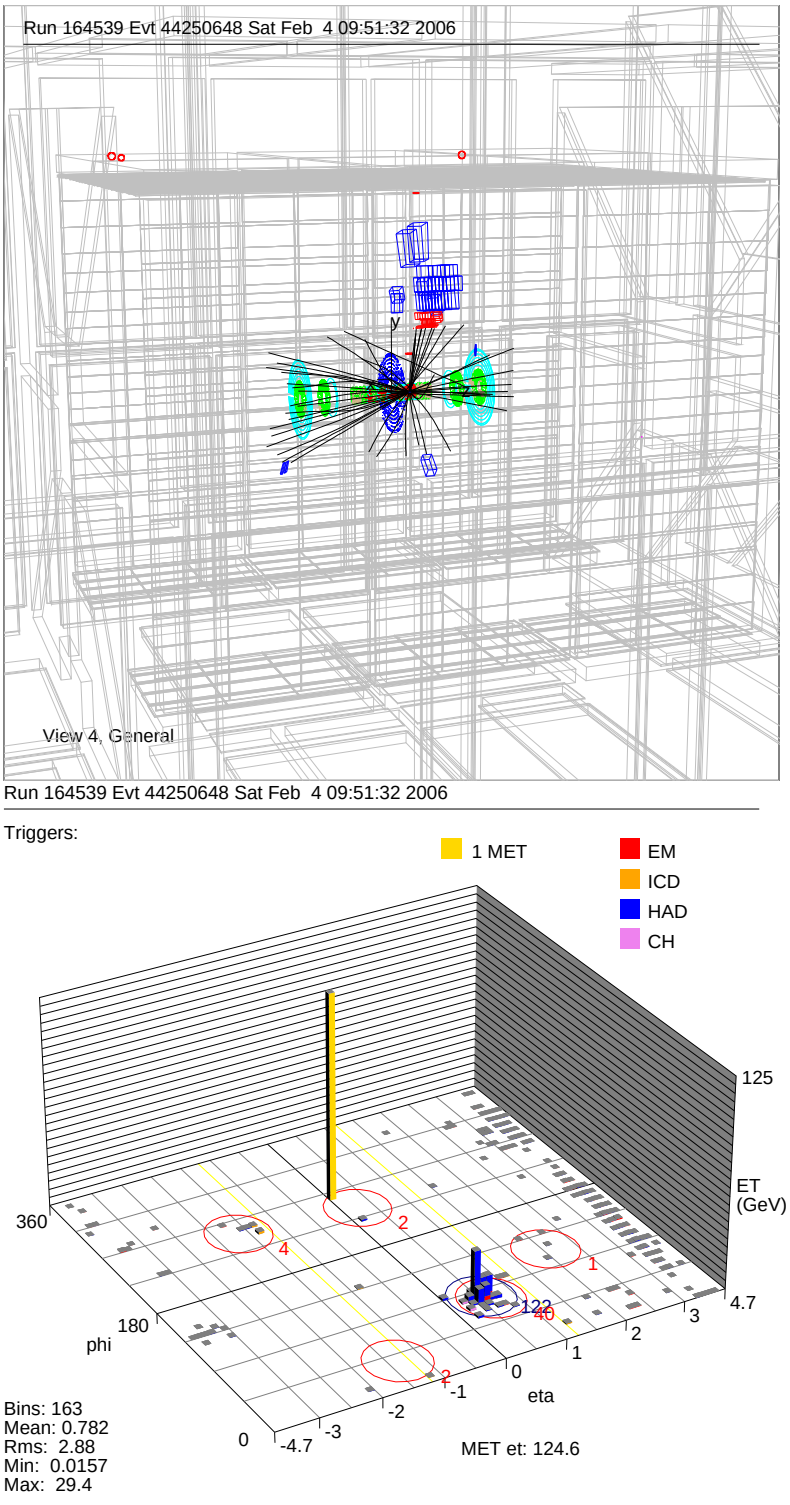

Figure 14: A typical diffractive event with a single observed jet.

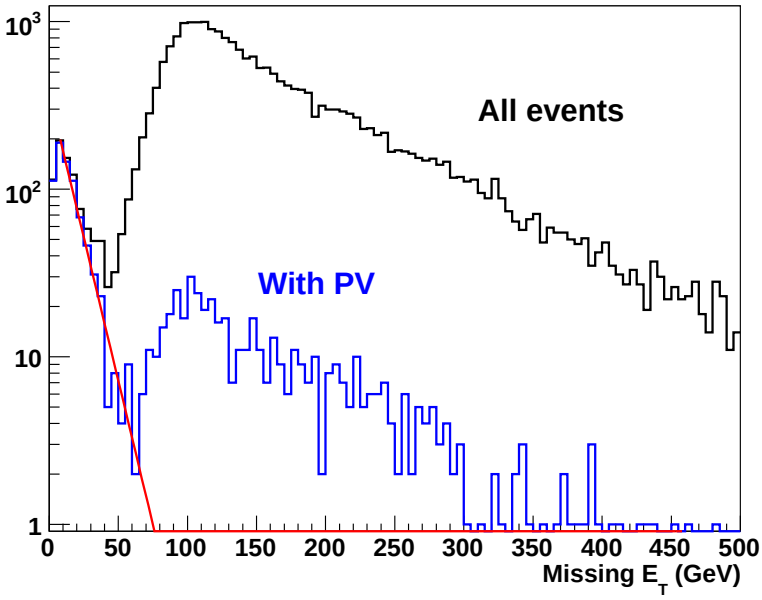

Figure 15: The $\not\!\!E_T$ distribution in events where the restriction of exactly one jet has been relaxed. The blue histogram is for the subset of events where a PV was found, and the black histogram is for all events. The red line is an exponential fit to the with-PV (blue) histogram for $\not\!\!E_T$<50GeV. Most of the events with small $\not\!\!E_T$ (<50 GeV) are understood to be diffractive events, as most of them have a reconstructed PV, and diffractive events are expected to have small $\not\!\!E_T$. The remaining events at large $\not\!\!E_T$ are understood to be mainly cosmic-induced showers, since most of these events do not have a reconstructed PV.

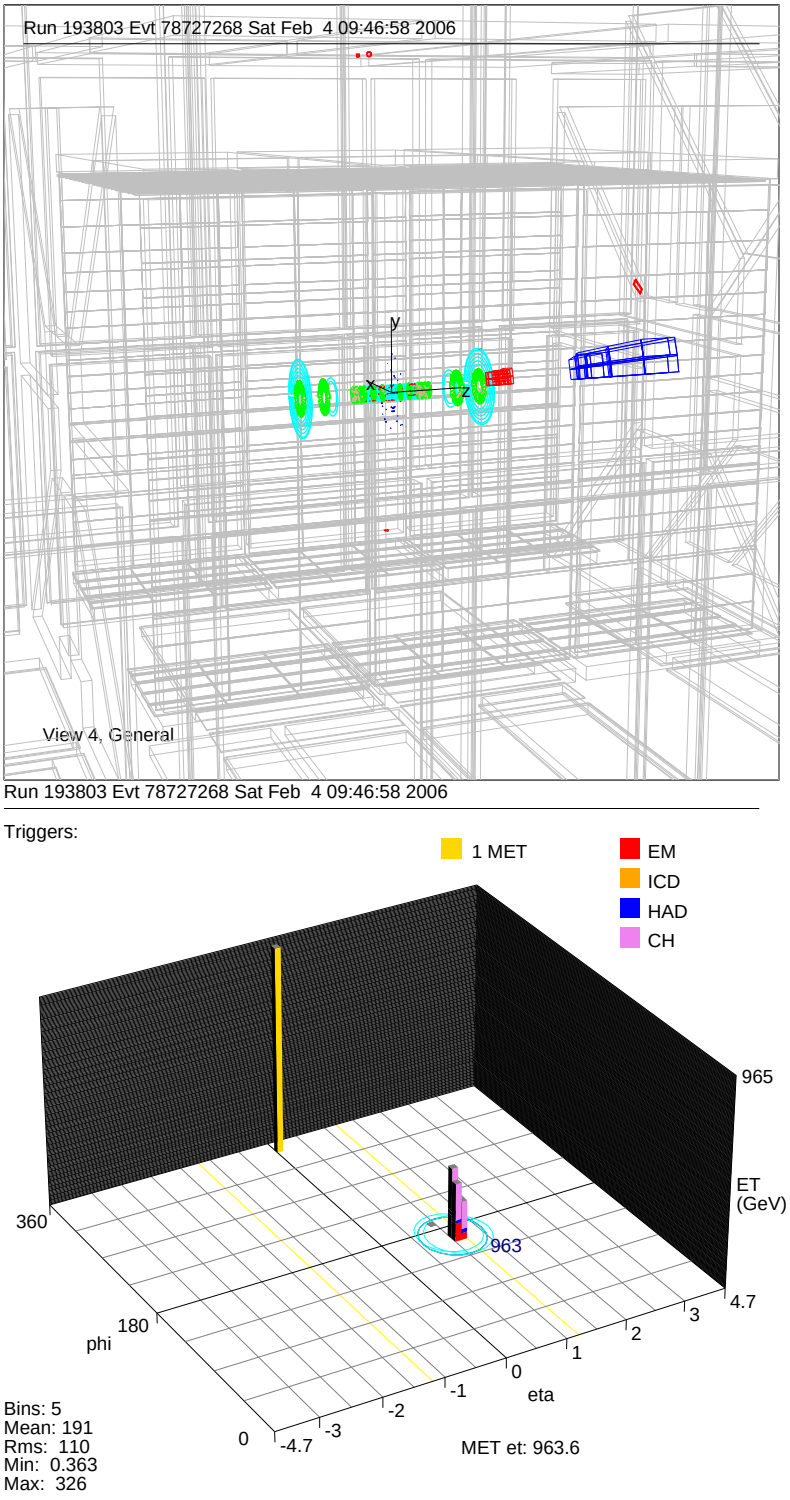

Figure 16: A detector problem event with a jet in a typical hot-spot. This hot region appears only in one run of the data set, and is also beyond the η<0.9 region used for analysis.

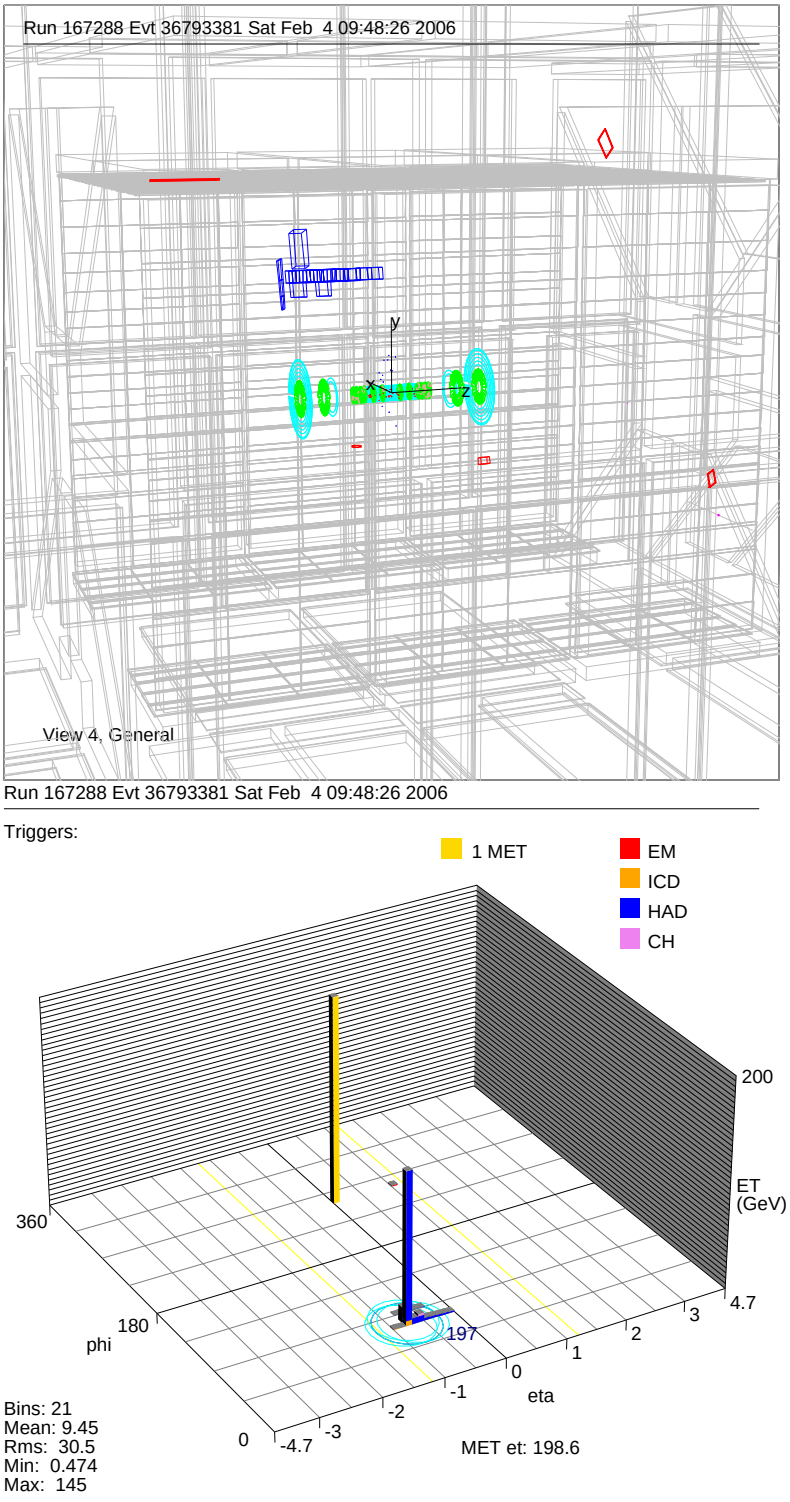

Figure 17: A detector problem event with a jet in a typical hot-spot. This hot region appears in many runs throughout the data set, and so is removed.

- Jet ϕ-width and η-width were both required to be <0.25 to eliminate events from certain types of detector problems, such as when pulsers were accidentally activated.

Further selections are then applied. The following criteria are used to select events containing "wide showers". (All jets which fail these cuts are considered "narrow showers" or "narrow jets".)

- Jet η-width and ϕ-width >0.08.
- Jet n90 >=10. This prevents fake wide showers from a narrow muon shower plus a long MIP trail.

These following criteria are used to select events containing "no-muon". (Events failing these criteria are considered "muon-jets" or "muon-events".)

- No $|NSEG| = 2$ or $|NSEG| = 3$ muons in the event. These events are nearly all cosmic muons (although we do lose about 10% efficiency here for gluino events).
- Require the $\Delta\phi$ between all pairs of A-layer ($|NSEG| = 1$) muons to be <1.5. Gluino jets often leak into the A-layer a bit, but we want to veto on back-to-back A-layer muons that could come from a single cosmic muon.
- Require the $\Delta\phi$ between any A-layer ($|NSEG| = 1|$) muon and the jet to be <1.5. We want to allow the jet to leak into the A-layer, but veto events where the A-layer muon is not associated with the jet (since it is then likely to be due to a cosmic muon).

A candidate gluino shower would be both wide and contain no muon, a so-called "wide no-muon shower". Figures 18 - 20 show displays of some of these candidate events. Figure 21 shows histograms of the properties of the candidates events.

8 Background Determination

To estimate the number of wide no-muon showers to expect from background (cosmic muon showers that happen to be wide and in which we happen to not see the muon), we use the assumption that the probability to not reconstruct the cosmic muon is independent of whether the muon shower is narrow or wide. Thus, we first measure the probability to miss the muon (P_{nomu}) in the narrow-jet cosmic data sample. Then this probability is applied to the wide-jet cosmic-muon data sample to predict the number (and energy spectrum) of wide-shower no-muon background events.

However, there are two complications that must first be dealt with in the narrow-jet sample before we can measure P_{nomu}. First, there are hot spots (detector problems / noise) that occur in the narrow-jet sample that are not manifested in the wide-jet data. This is understandable, since many detector problems and noise can be isolated to a single calorimeter cell or a small group of cells, and thus would lead only to narrow fake jets. These hot spots are removed from the narrow-jet sample before P_{nomu} is

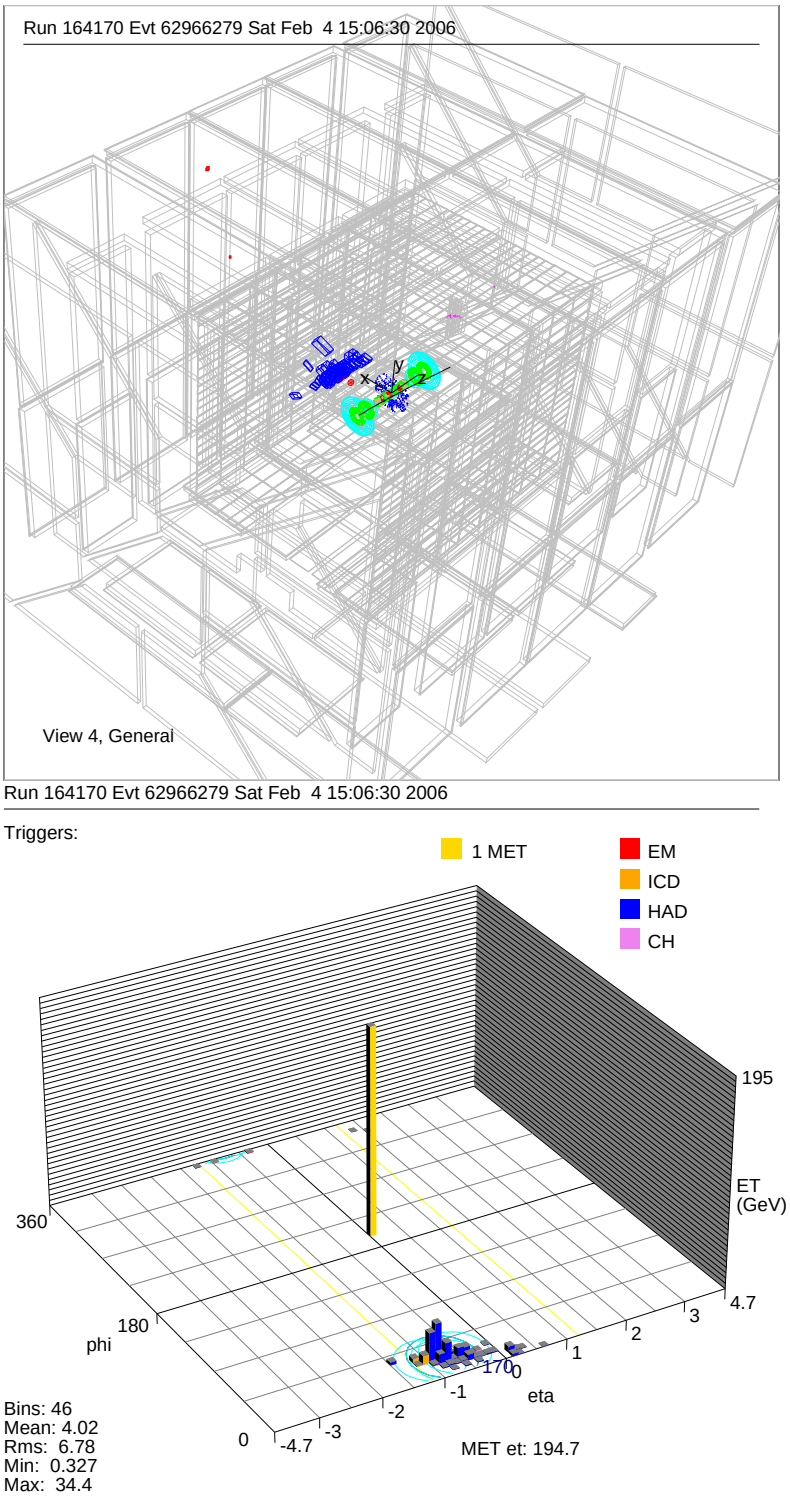

Figure 18: A typical candidate signal event, a wide shower, with no good muon.

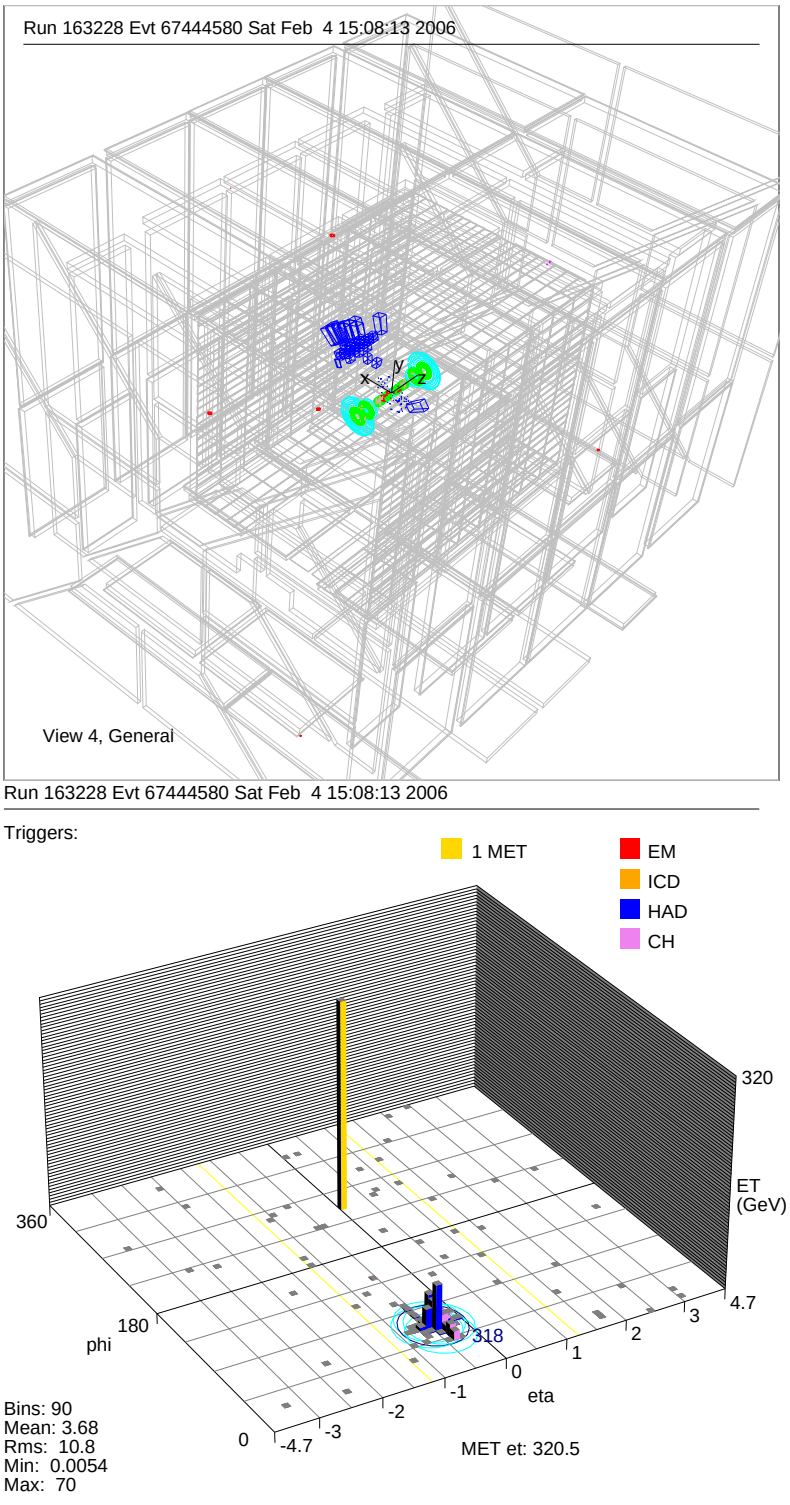

Figure 19: A typical candidate signal event, a wide shower, with no good muon.

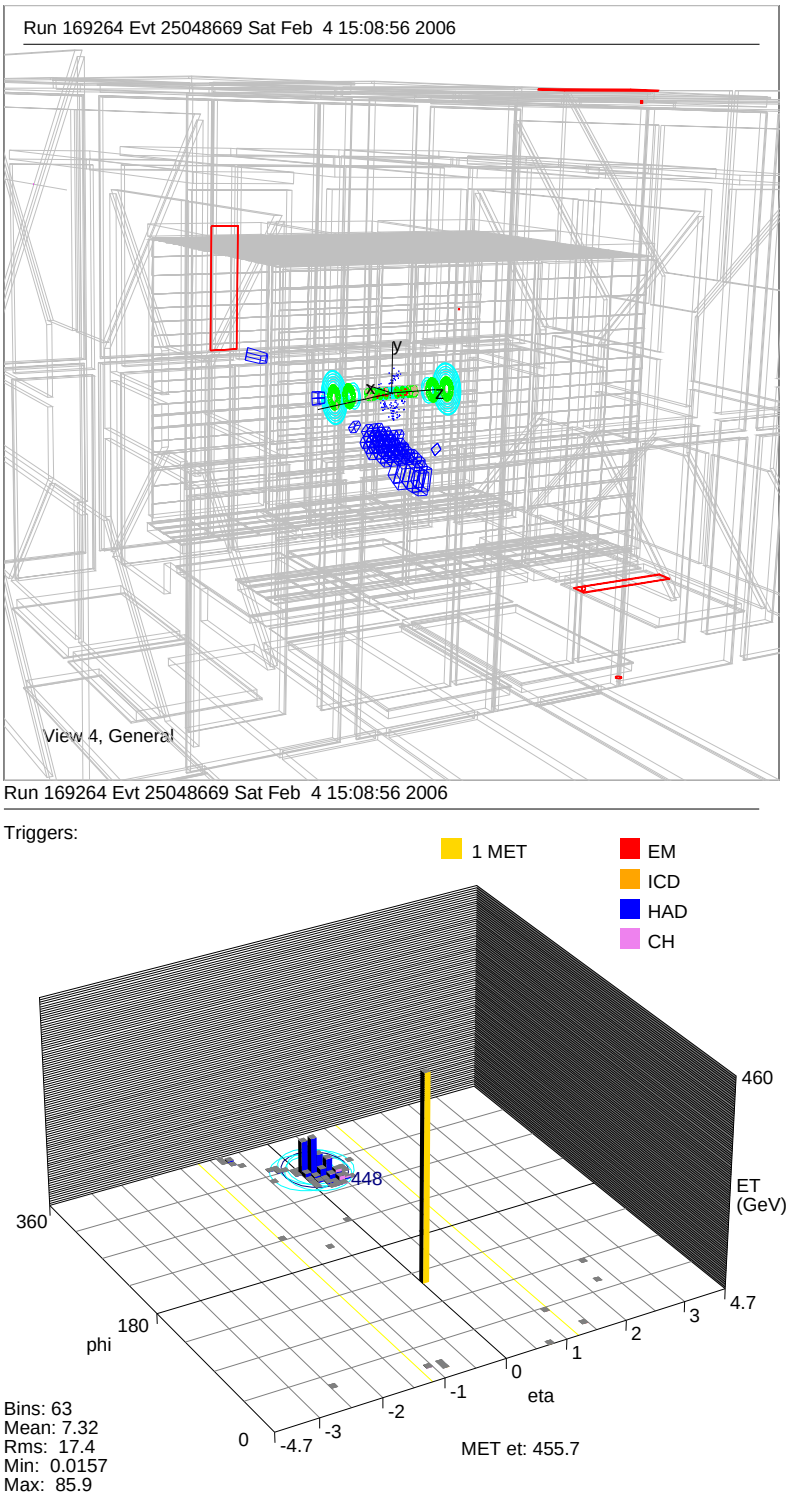

Figure 20: A typical candidate signal event, a wide shower, with no good muon.

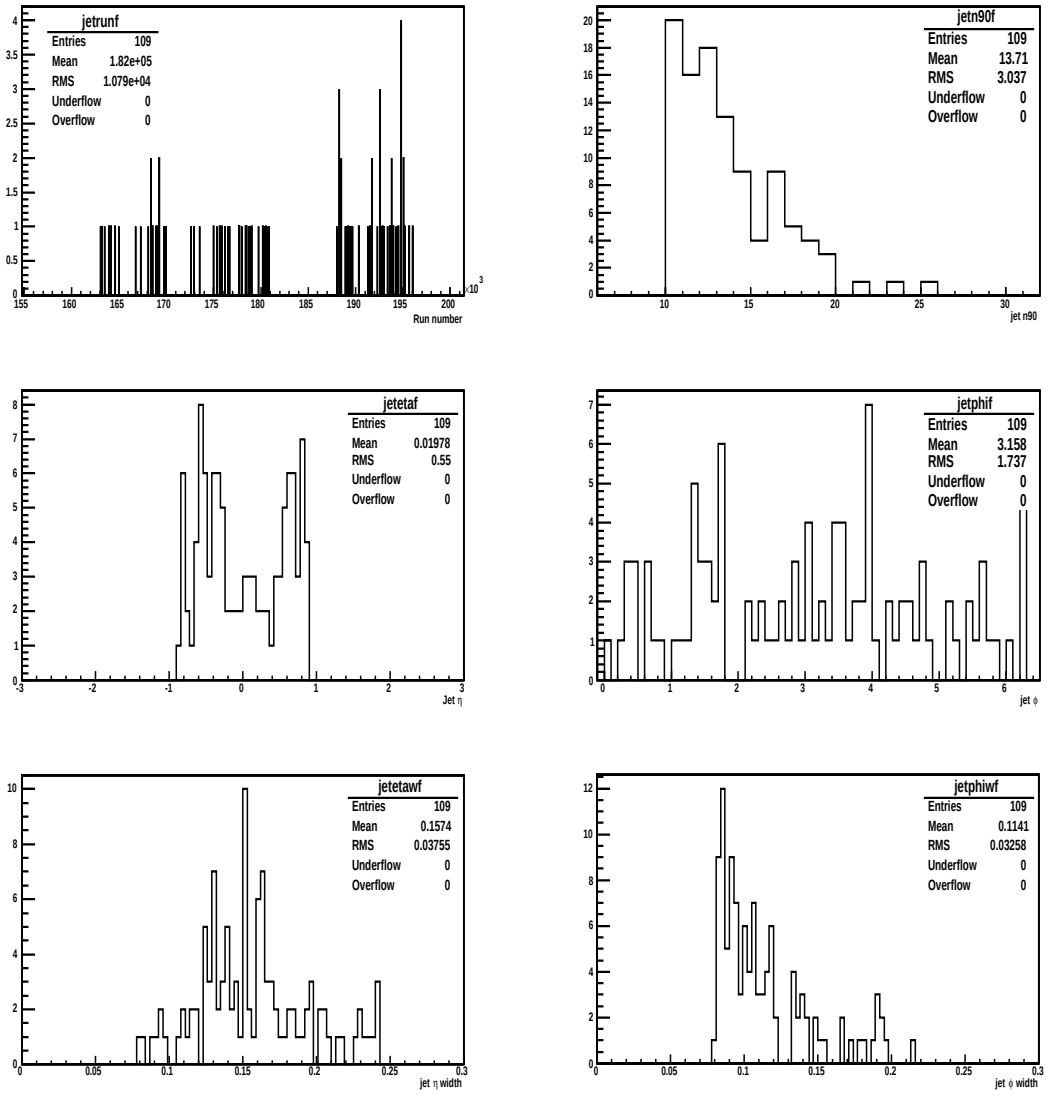

Figure 21: The properties of the candidate events, those with a wide-jet shower and no-muon. From left to right and top to bottom, the run number of the event, the jet n90, η, ϕ, η-width, and ϕ-width.

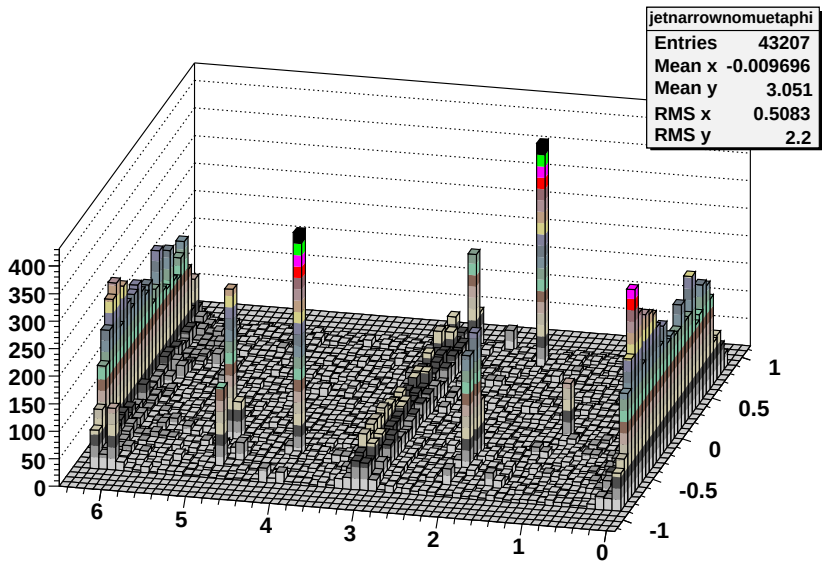

Figure 22: A histogram of the narrow-jet η vs. ϕ, showing the hot spots present for the narrow-jets, as well as the ridges from beam-muons.

measured, using the following procedure. A 2-dimensional histogram is made of the narrow-jet phi vs. eta, as shown in Figure 22. We can see that there are at least 5 regions that are very "hot". And we also observe the pattern of beam-muons that exist near integer multiples of ϕ/π (in the plane of the beam). Since we wish to remove both these sources of narrow-jets (further methods are discussed below to deal with the remaining beam-muon-induced narrow-jets), hot regions of this histogram will be excluded. Any bin with more than 50 entries is considered a "bad" region, and is excluded when measuring P_{nomu}. The resulting phi vs. eta distribution after this cut is shown in Figure 23.

The second issue to be dealt with in the narrow-jet sample, as already alluded to, is that there is contamination from beam-muons. The beam-muon events have different properties than the cosmic showers, due to their production mechanism and the angle that they tend to enter the detector from. Their energy spectrum is different from the cosmic showers, and falls off faster with energy (for instance, there are no showers above 1 TeV!). Because they enter parallel to the beam-line, they can not readily induce showers with large ϕ-width, so they do not contribute significantly to the wide-jet events. And since they preferentially enter the detector near the far-forward region where muon acceptance is smaller, it is more likely to not reconstruct the muon in beam-muon events. For all of these reasons, it is critical to remove the contribution from beam-muons when measuring P_{nomu}.

We can use the fact that the energy spectrum is softer for beam-muon events in order to separate them from cosmic-muon events. If we plot P_{nomu} as a function of jet energy, as in Figure 24, we see that P_{nomu} decreases vs. energy to a plateau of about 10%. The hypothesis is that beam-muons cause P_{nomu} to be larger at low energy, and evidence for this will now be shown. We can fortunately study the properties of

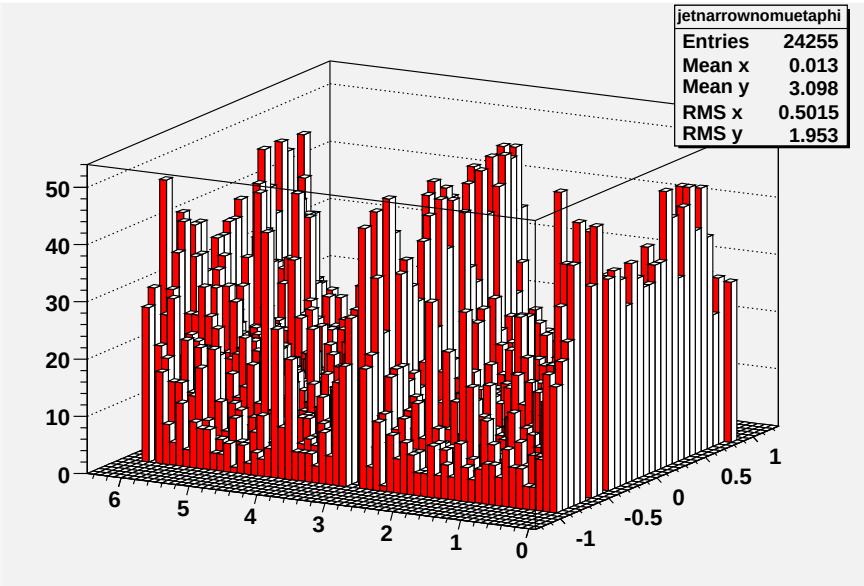

Figure 23: A histogram of the narrow-jet η vs. ϕ after cutting at 50 entries, showing that the hot spots present for the narrow-jets have been removed. Some of the ridges from beam-muons remain.

nearly-pure beam-muon showers whenever we do reconstruct the muon, since this muon is in-time ($|\Delta t|$<10ns) and the shower is near the plane of the beam, as shown in Figure 25. If we plot the fraction of in-time muons vs. energy, as in Figure 26, we see that the fraction decreases steadily vs. energy towards a plateau of about 5%. If the muons were all of cosmic origin, and thus flatly distributed in time, the fraction of muons that randomly happened to be in-time would be 20ns / 396ns = 5%. (The $|\Delta t|$<10ns criteria implies a time window for in-time muons a total of 20ns wide.) Thus, at high energy (above 400 GeV), there is a negligible contribution from beam-muons. So we can measure P_{nomu} in the region above 400 GeV, as was shown in Figure 24, and arrive at P_{nomu}=0.11$\pm$0.01.

9 Signal Efficiency

To first order, the detection efficiency for the stopped gluino signal events can be estimated from the MC simulation. The fraction of events falling outside the jet energy cuts, $|\eta|$ cut, n90 cut, and jet η-width and ϕ-width cuts can be fairly accurately predicted. Table 1 shows the efficiency for each criteria.

Some effects are not modeled in the MC, however. For instance, there is a loss of efficiency at the trigger level from the GAPSN requirement. If a min-bias event happens to occur during the bunch crossing when the gluino decays, the GAPSN trigger will not fire. The fraction of the time this occurs has been measured using cosmic-muon shower events [5] triggered on the JT_125TT trigger from the "QCD" skim. It is observed that

[5]These are mostly narrow-jet showers, but no explicit requirement on the shower was made. The cosmic muon requirement means that the muon had timing information, and it was "out-of-time"

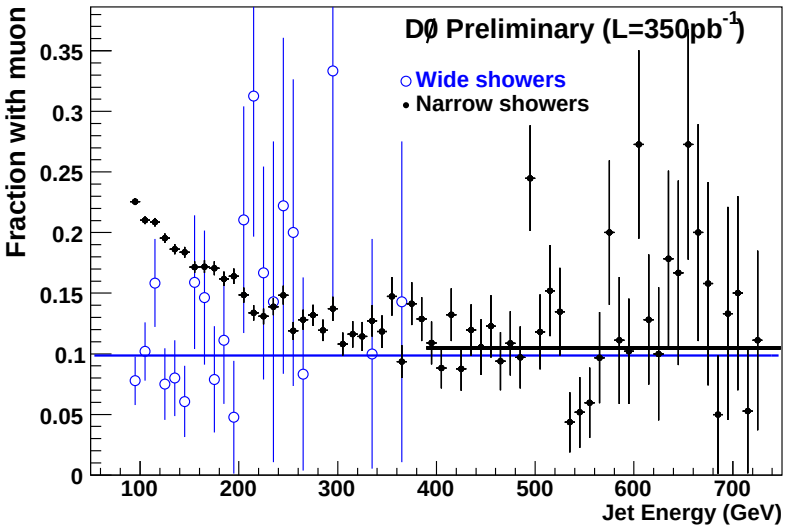

Figure 24: The ratio of the number of wide (blue circles) and narrow showers (black dots) with muons to the number without muons, vs. jet shower energy. Also shown are the fits (to constants) to both distributions.

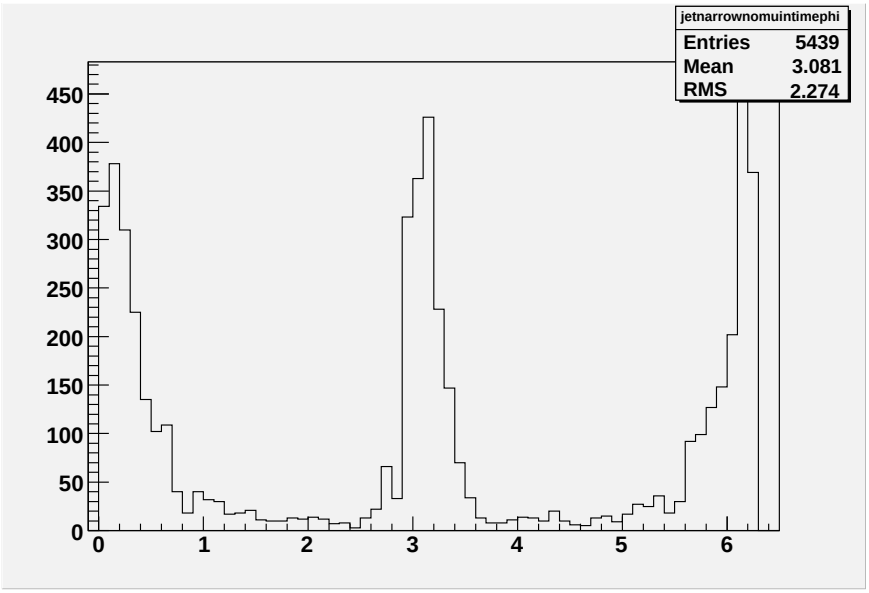

Figure 25: The ϕ distribution of in-time A-layer muons in narrow-jet showers.

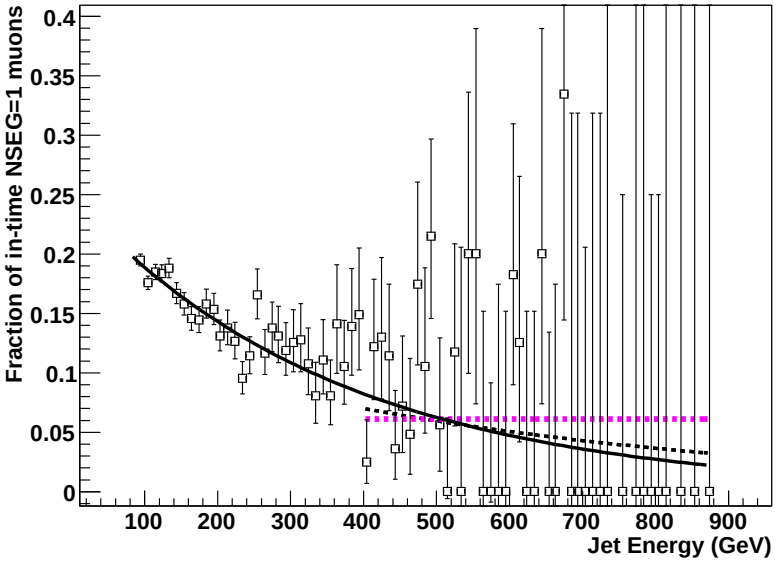

Figure 26: The fraction of in-time A-layer muons in narrow-jet showers, vs. jet shower energy. The solid curve is an exponential fit across the entire energy range. The dotted fits are exponential and constant fits above 400 GeV.

Sample	1 Jet	$\|\eta\|$	E>90	No PV	W.<.25	W.>.08	n90	No mu
200	0.91	0.91	0.17	0.93	1.00	0.71	0.70	1.00
300	0.88	0.89	0.48	0.97	1.00	0.51	0.88	0.99
400	0.83	0.90	0.60	0.97	0.99	0.56	0.88	0.98
500	0.82	0.91	0.64	0.97	0.99	0.58	0.85	0.96

Table 1: The signal efficiencies for each cut, for each simulated gluino mass sample.

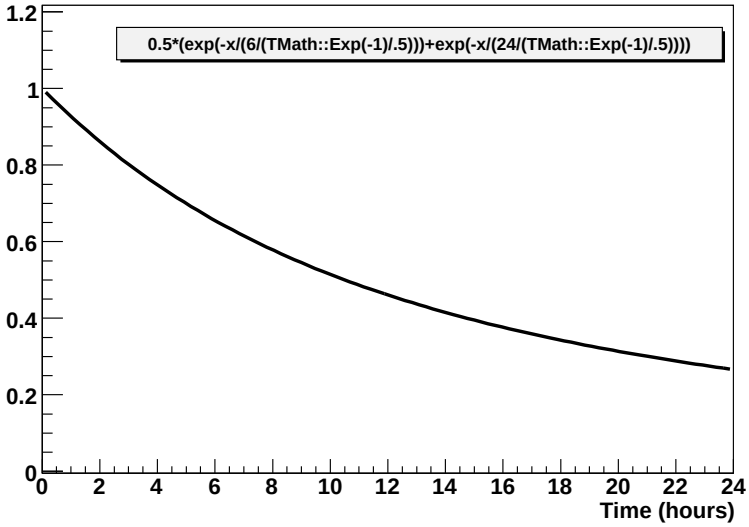

Figure 27: The typical luminosity profile of a store.

75% of the time that JT_125TT fired, the JT_45TT_GAPSN trigger also fired, thus the efficiency of the GAPSN trigger term, for cosmic-muon showers, averaged over the PASS2 data set, is 75%. The probability to have no min-bias interactions during a given crossing is proportional to $e^{-\lambda}$, where λ is the average number of interactions per crossing, which is proportional to the instantaneous luminosity. For this data set, $\lambda \simeq 0.30$, since this number gives the observed average GAPSN efficiency.

A more detailed model has also been made of the trigger efficiency as a function of the gluino lifetime. First, the typical store's instantaneous luminosity profile has been modeled, as shown in Figure 27. For each MC event, the production time is chosen randomly, according to this store distribution. The decay time is then chosen randomly according to the production time plus a random decay time chosen from the exponential decay distribution corresponding to the gluino lifetime. Since it is possible that the store has ended if the decay occurs many hours after the store began, the following model is used. A store is assumed to last 24 hours, and there is a 50% chance of another store occurring 6 hours later. This is a reasonable fit to the Tevatron operations during which the data was taken. The details of the store model will start to have an impact only for gluinos with a long lifetime (>3 hours). If a store is determined to be ongoing, the GAPSN efficiency is then estimated according to the *current instantaneous luminosity at the decay time*. The GAPSN efficiency is assumed to be the probability of having no min-bias interaction, which according to the Poisson distribution is $e^{-0.3*lum}$. *lum* is the current instantaneous luminosity divided by the average instantaneous luminosity, again derived from the store profile of Figure 27. The average number of min-bias interactions is directly proportional to the instantaneous luminosity. The final average GAPSN efficiency for a stopped gluino is shown as a function of the gluino lifetime in Figure 28. (For reference, the efficiency assumed for

with the bunches. This is rejection against beam-muons.

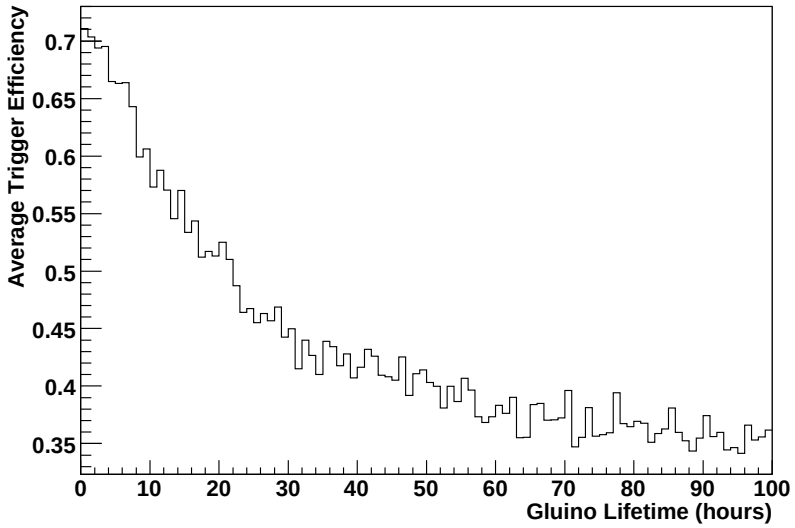

Figure 28: The average GAPSN efficiency for a stopped gluino, as a function of the gluino lifetime.

Source	Efficiency
GAPSN Trigger	.7 (for small gluino lifetime)
Trigger gaps	.68
Total	0.48

Table 2: The extra signal inefficiencies, and their total product.

the preliminary results was simply $60 \pm 15\%$, and the gluino lifetime was assumed to be <3 hours.)

Another source of inefficiency is that the trigger is not live all the time, but only during the "live super-bunches", see Figure 29. During the sync-gap and each of the two cosmic-gaps, the triggers are dead [6]. The live super-bunches make up 68% of the total accelerator turn time, with minimal uncertainty.

Table 2 shows the additional sources of inefficiency and the total efficiency to be multiplied by the MC acceptance. The final signal efficiencies will be shown in Table 4.

[6] A trigger which fires during the cosmic gaps (21% of the turn) is under discussion for future use. It is not possible for DØ to trigger during the sync gap (11% of the turn), when crate electronics are performing other tasks.

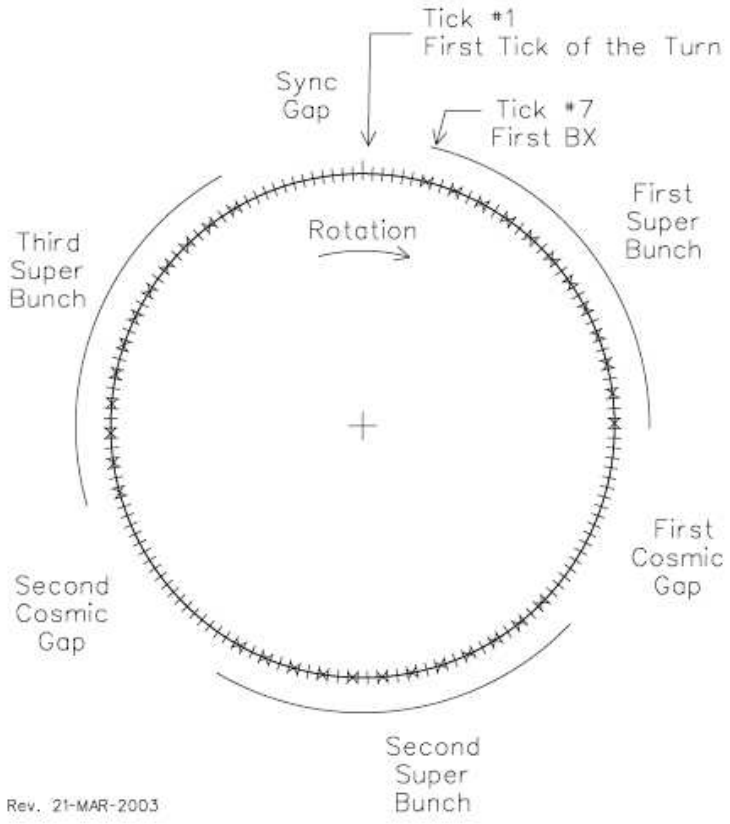

Figure 29: The Tevatron bunch structure. (Thanks to Dan Edmunds.)

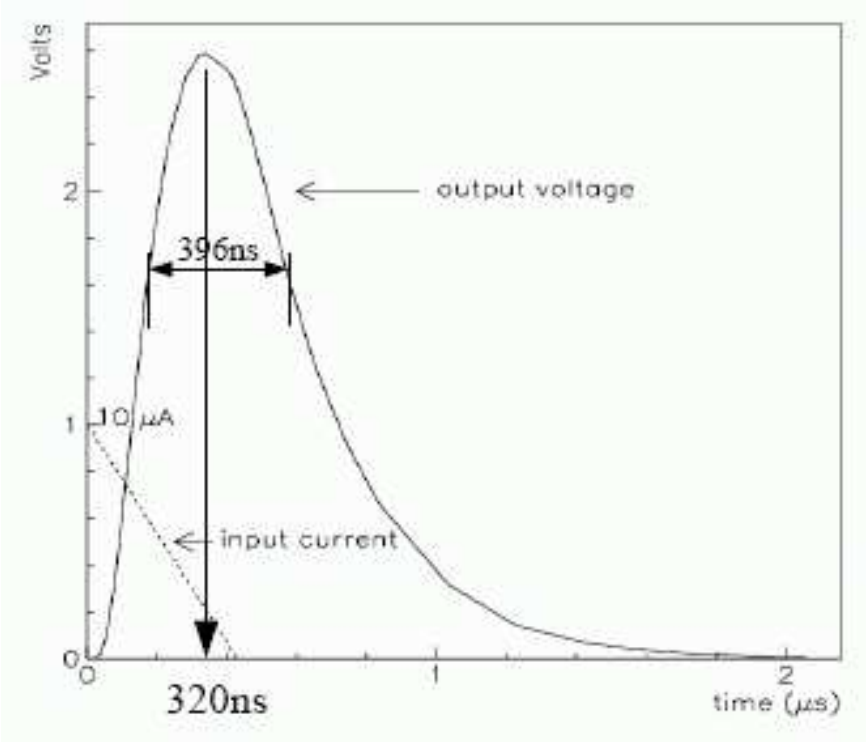

Figure 30: The timing of the calorimeter precision readout.

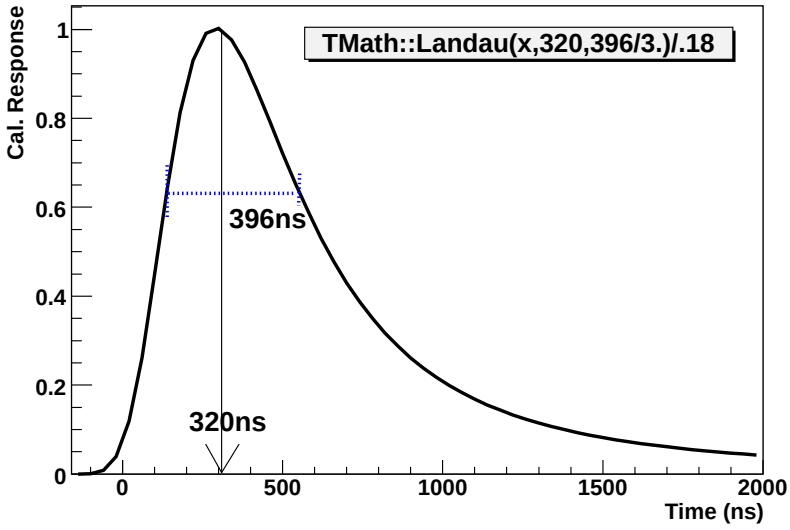

Figure 31: The model of the calorimeter precision response used.

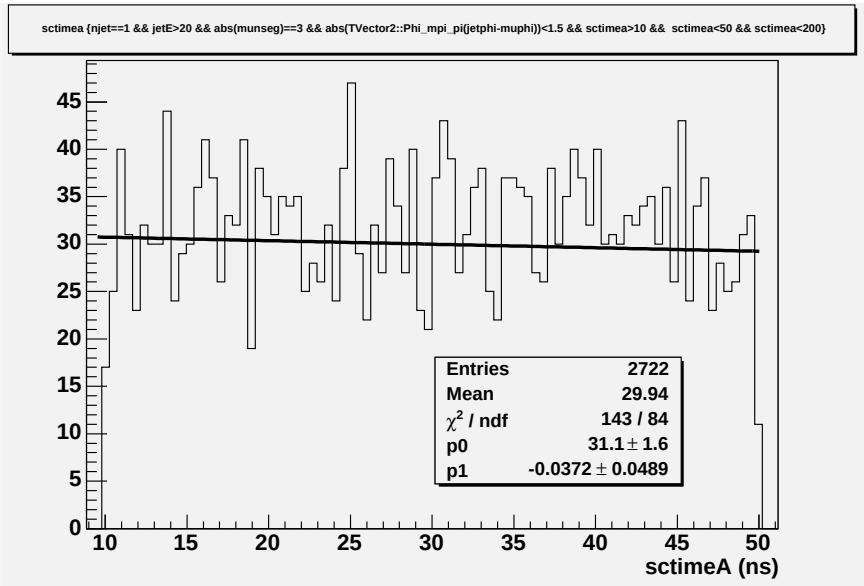

Figure 32: The number of muon showers above threshold vs. the muon scintillator time.

Finally, there is also a shift of the observed jet energy towards lower energies whenever the calorimeter signal from the gluino decay is not in-time with the bunch-crossing time. This is due to the fact that the calorimeter electronics samples the shaped calorimeter signal only once, at the assumed peak of the signal, assuming that the signal is a maximum near the start of the bunch crossing (when ions begin to drift), see Figure 30. The effect can be studied in data by looking at cosmic-muon showers where the muon has been reconstructed. Unfortunately, very little difference can be seen vs. the muon time, as seen in Figure 32, since the time window (up to only 50ns [7]) is short compared to where efficiency should start to drop (around 140ns).

A rather detailed model of the calorimeter response is made, which will also approximate the *spread* of jet response. The calorimeter response is modeled with a Landau function, which approximates the response measured via pulse injection for the Run II calorimeter shapers, as shown in Figure 31. For each simulated jet, this model of the response is sampled, and the jet energy is corrected (downwards) accordingly. When to sample the response depends upon when the event is triggered. The L1 calorimeter trigger uses a separate set of shapers, and thus has a different response curve, which is *faster* to rise than the precision response. (The trigger was designed to operate at 128 ns bunch crossing!) If a signal is >100 ns late, the following bunch crossing is triggered on because the trigger threshold (usually 2 towers above 3 GeV) was not reached. Whereas if the event is <100 ns late the current bunch crossing will be triggered. We thus sample the precision response curve randomly from 320-100 ns to 320+296 ns. A last consideration is that the precision response from the previous bunch crossing is always subtracted from the current crossing's measurement, in a process known as "baseline subtraction". This serves to limit the increase in calorimeter

[7] The muon scintillator time window is limited by the muon readout electronics.

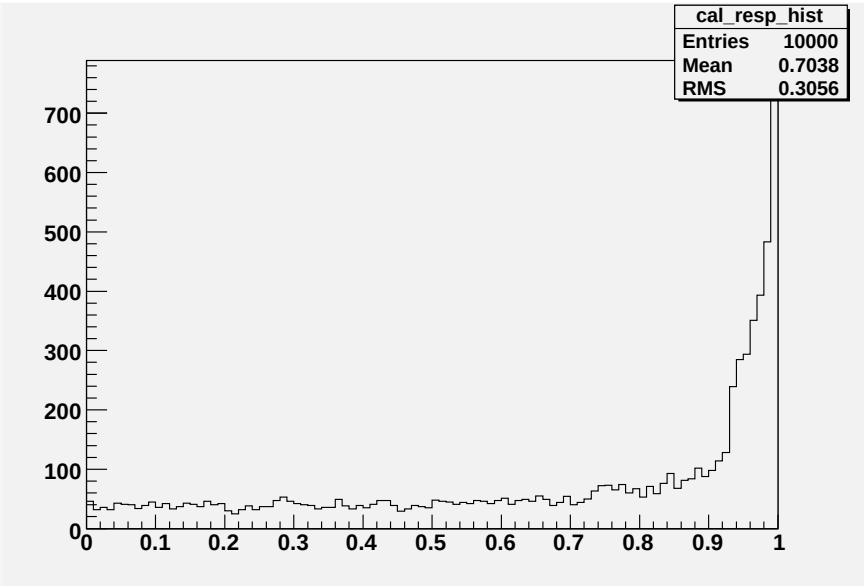

Figure 33: The distribution of corrections applied to the jet energy for jets in the 400 GeV simulated stopped gluino sample. Note that the average estimated correction value, 85.5% is in excellent agreement with that measured in data from cosmic muons.

energy with increased instantaneous luminosity due to pile-up interactions. Our model of the calorimeter response takes baseline subtraction into account by subtracting the sampling 396 ns earlier from the current sampling. Since the sampling will be 0 for times less than 320 ns, this correction only affects events which were late enough to be triggered on the following crossing (about 2/3 of events). The final distribution of corrections due to the out-of-time calorimeter response, for a distribution of jet energies from the 400 GeV simulated gluino sample, is shown in Figure 33.

10 Systematic Uncertainties

Several sources of systematic uncertainty have been identified. They fall into two general categories: errors affecting the calculation of signal acceptance and those that affect the number of estimated background events. The errors from all sources which affect the signal acceptance are added in quadrature. Table 3 shows the sources of uncertainty, and their total.

The first signal acceptance uncertainty is due to the modeling of the signal by the MC simulation. The error on the shift in average shower energy caused by the out-of-time calorimeter signals will be taken as 30% relative, equal to a $\pm 5\%$ absolute energy shift. Varying the jet energy within this range changes the total efficiency by 8-12%, depending on the signal sample (less variance for larger gluino mass). Varying the jet energy within the uncertainties on the data/MC jet energy scale changes the total efficiency by 5-9%. Most jets are well above the 90 GeV energy threshold. Also, shifting the energy scale causes nearly as many jets to fall below the lower window cut as below the upper window cut (see below for a description of the window cut

Source	Uncertainty (%)
Out-of-time Response	12
Data/MC Jet Energy Scale	9
η Distribution	9
Radial Distribution	7
Other Geometrical/Kinematic Acceptance	5
GAPSN Trigger Efficiency	5 (up to 15)
Total	20 (up to 25)

Table 3: The systematic uncertainties on signal efficiency, and their total (added in quadrature).

for signal selection). Varying the $|\eta|$ cut by ± 0.1 changed the efficiency by 9%, which is a good estimate of the variance due to the η distribution of the stopped gluinos. Varying the assumed cross-section for R-hadron neutral to charged conversion when passing through matter changes the expected radial distribution of the stopped gluinos, as seen in Figure 1. The signal efficiency changed by -4% and -7% when varying the cross-section to 30mb and 0.3mb, respectively. There is also some uncertainty from the MC modeling itself, estimated to be 5%, from various other sources such as jet shape, for instance.

Another signal acceptance uncertainty is the efficiency due to the GAPSN trigger requirement. Variations of the number of primary vertices expected per event, the modeling of the store luminosity profile, and (for large gluino lifetimes) the between-store Tevatron operations can vary the efficiency by up to 5-15%, depending on gluino lifetime (larger uncertainty for larger lifetime).

There is an uncertainty arising from the limited statistics in the narrow-jet no-muon data sample, resulting in a 10% uncertainty on the normalization of the expected background.

The systematic uncertainty on the integrated luminosity is 6%, or about 20pb^{-1}.

11 Results

If we apply the measured P_{nomu} to the wide-jet cosmic-muon data sample, we can estimate the energy spectrum of the expected wide-jet no-muon background, as shown in Figures 34 and 35 along with the observed wide-jet no-muon events in data. The estimated background predicts the data well, and there is little excess in data at any energy range, as seen in Figure 36, where the expected background has been subtracted from the data.

Given an observed number of candidate events, an expected number of background events, and a signal efficiency in a certain jet energy bin, we can exclude at 95% C.L. a calculated rate of signal events giving jets of that energy, taking systematic

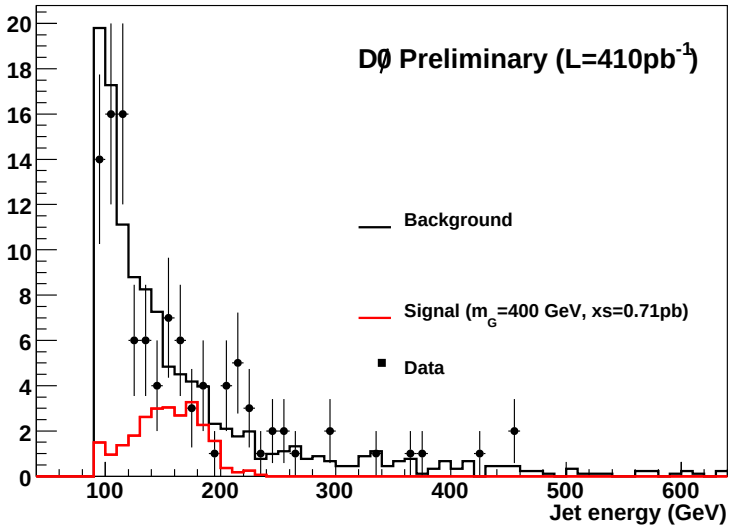

Figure 34: A comparison of the wide-jet no-muon data to the expected background. Also shown is the signal simulated for m_G=400 GeV and m_{LSP}=90 GeV at the excluded limit of 0.7 pb (in red), for a small gluino lifetime (<3 hours).

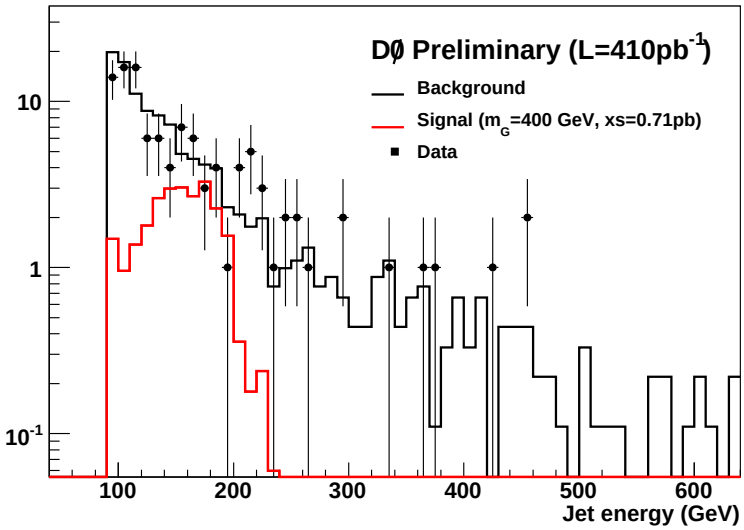

Figure 35: A comparison of the wide-jet no-muon data to the expected background, with log scale. Also shown is the signal simulated for m_G=400 GeV and m_{LSP}=90 GeV at the excluded limit of 0.7 pb (in red), for a small gluino lifetime (<3 hours).

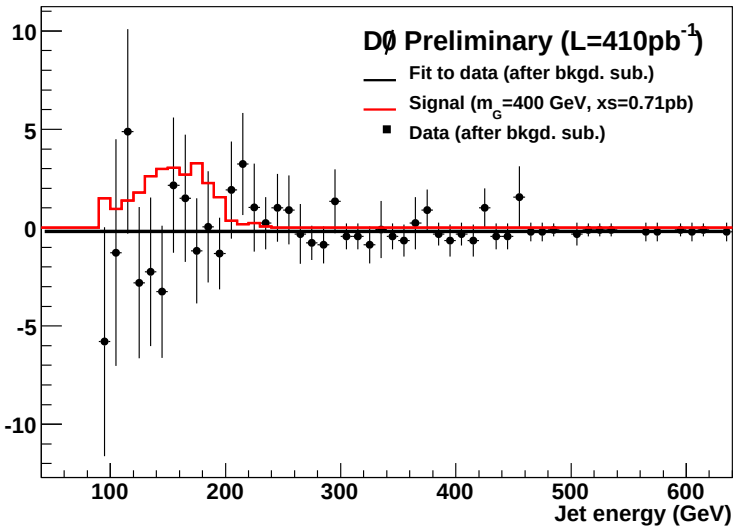

Figure 36: The wide-jet no-muon data, after subtracting the expected background. Also shown is the signal simulated for m_G=400 GeV and m_{LSP}=90 GeV at the excluded limit of 0.7 pb (in red), for a small gluino lifetime (<3 hours).

uncertainties into account [8]. This is a fairly model-independent result, limiting the rate of any out-of-time mono-jet signal of a given energy. From there one could derive limits in the plane of $M_g - M_{LSP}$ for a specific stopped gluino model.

The jet energy ranges chosen are calculated from the resolution of the simulated MC samples. The signal window for each of the four samples is from M-0.5*RMS to M+2.0*RMS, where M is the sample's jet energy mean (after all selections) and RMS is the sample's jet energies' RMS. Approximately 80% of the simulated signal events fell within this window cut, depending weakly on the signal mass. An asymmetric window was chosen since the background is falling exponentially with increasing jet energy, whereas the signal is roughly symmetric in jet energy around the mean. Table 4 shows, for each jet energy range considered, the number of events observed in data, expected from background, the signal efficiency (for a small gluino lifetime, <3 hours), and the corresponding observed and expected [9] cross-section limits on signal jets. The integrated luminosity was 410±20 pb^{-1}, as calculated in Section 3. These results are also shown in Figure 37.

From the relation between the gluino and LSP masses and the observed jet energy, Equation 1, one can solve for the gluino mass:

$$M_g = E + \sqrt{E^2 + M_{LSP}^2} \tag{2}$$

Using this equation, results can be translated from the generated set of signal samples

[8] The Bayesian limit setting routing "CL95" in the CVS package "limit_calculators" has been used.

[9] The expected limit is calculated by setting the number of "observed" events to the number of expected events from background. It is the limit that would be derived in the average experiment if there were no signal.

Jet E Range (GeV)	Data	Bgnd.	Eff.	Exp. Limit (pb)	Obs. Limit (pb)
92.5-104.6	30	37.07	0.017	2.61	1.81
112.4-156.6	39	40.26	0.049	0.94	0.89
141.3-213	34	30.91	0.068	0.56	0.71
168.7-270.6	32	25.74	0.072	0.48	0.75

Table 4: The data, background, efficiency, and observed and expected limits (at 95% C.L.) for each jet energy range. (The efficiency is for a small gluino lifetime, <3 hours.)

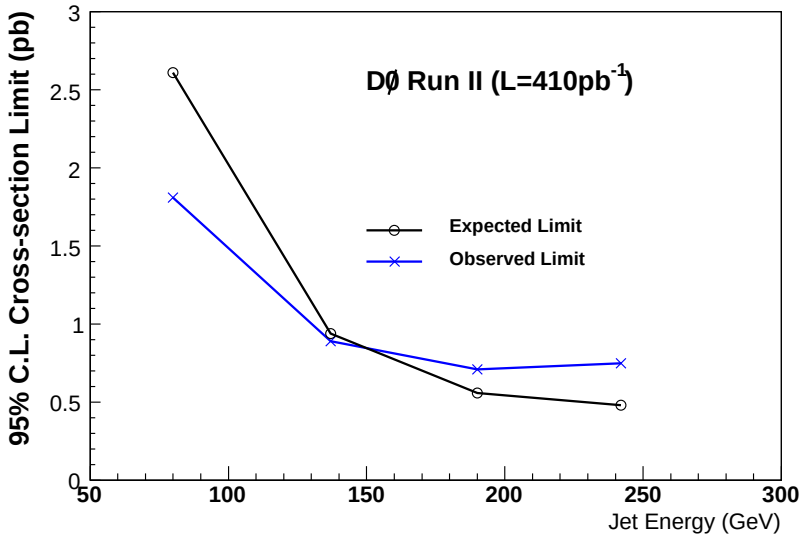

Figure 37: The 95% C.L. upper limits expected (black, open circles) and observed (blue, filled circles) on the cross-section of stopped particles decaying into a jet within various energy ranges.

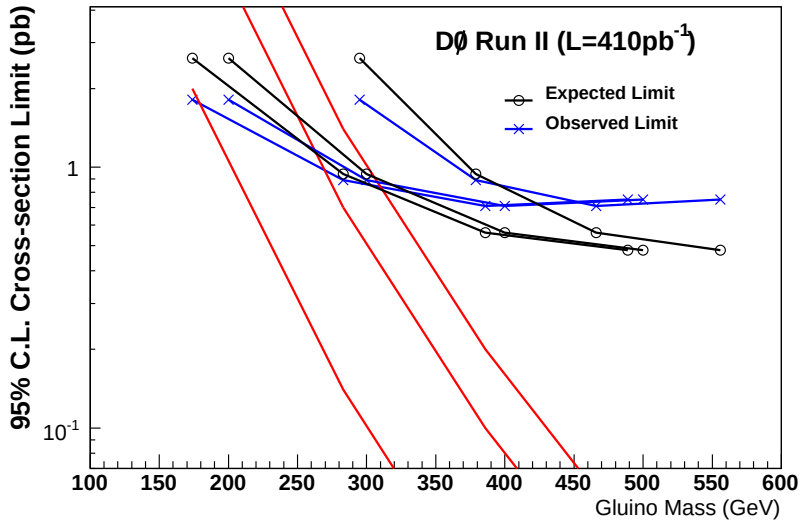

Figure 38: The 95% C.L. upper limits expected (black, open circles) and observed (blue, crosses) on the cross-section of stopped gluinos decaying into a jet, assuming a 100% BR of G→g+LSP and a small gluino lifetime (<3 hours). The various curves correspond to the 3 choices of the simulated LSP mass: 50, 90 and 200 GeV, from left to right. Also shown is the theoretical cross-section (red, stars), from [3], for conversion cross-sections of 0.3, 3, and 30 mb.

to any other set of (M_g,M_{LSP}) which would give the same generated parton (jet) energy. For example, one of the generated samples had M_g=400 GeV and M_{LSP}=90 GeV (all of the generated samples had M_{LSP}=90 GeV, which corresponds to the Z mass). This corresponded to a parton (jet) energy of 190 GeV, as given by Equation 1. If instead M_{LSP} had been chosen to be 200 GeV, an equivalent jet energy could have been simulated by having M_g be 466 GeV, according to Equation 2. We can now place upper limits on the stopped gluino cross-section for a given LSP mass, assuming a 100% BR of G→g+LSP. These can be compared with the predicted cross-sections for stopped gluinos (which includes its production and its probability to stop) taken from [3]. Tables 5, 6, and 7 show the gluino cross-sections excluded for assumed LSP masses of 50, 90, and 200 GeV, respectively, for a small gluino lifetime (<3 hours), compared to the theoretical predictions (for a conversion cross-section of 3mb). These results are also shown in Figure 38, where the limits are compared to theoretical cross-sections for conversion cross-sections of 0.3, 3, and 30 mb.

If the gluino lifetime is significantly longer (on the scale of the typical store luminosity profile), the efficiency of the trigger degrades, as shown in Figure 28. The resulting effect on the stopped gluino cross-section limits for an LSP mass of 50 GeV is shown in Figure 39.

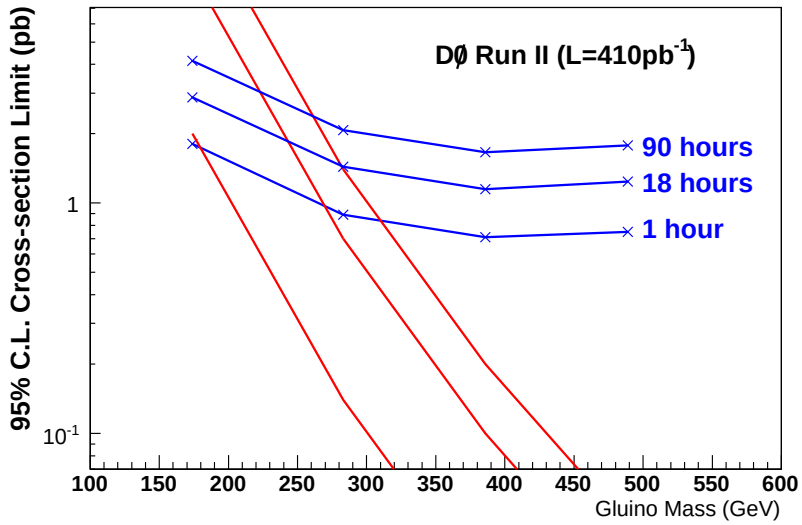

Figure 39: The 95% C.L. upper limits observed on the cross-section of stopped gluinos decaying into a jet, for various assumptions of the gluino lifetime: 1, 18, and 90 hours, for an LSP mass of 50 GeV, assuming a 100% BR of G→g+LSP. The longer the gluino lifetime, the weaker are the cross-section limits. Also shown is the theoretical cross-section (red, stars), from [3], for conversion cross-sections of 0.3, 3, and 30 mb.

Jet E (GeV)	Gluino Mass (GeV)	Observed Limit (pb)	Theoretical CS (pb)
80	174	1.81	10
137	283	0.89	0.7
190	386	0.71	0.1
242	489	0.75	0.02

Table 5: The gluino mass, observed cross-section limit, and the theoretical cross-section for each jet energy, assuming an LSP mass of 50 GeV, assuming a 100% BR of G→g+LSP and a small gluino lifetime (<3 hours).

Jet E (GeV)	Gluino Mass (GeV)	Observed Limit (pb)	Theoretical CS (pb)
80	200	1.81	5
137	300	0.89	.5
190	400	0.71	.05
242	500	0.75	.01

Table 6: The gluino mass, observed cross-section limit, and the theoretical cross-section for each jet energy, assuming an LSP mass of 90 GeV, assuming a 100% BR of G→g+LSP and a small gluino lifetime (<3 hours).

Jet E (GeV)	Gluino Mass (GeV)	Observed Limit (pb)	Theoretical CS (pb)
80	295	1.81	.5
137	379	0.89	.07
190	466	0.71	.03
242	556	0.75	.005

Table 7: The gluino mass, observed cross-section limit, and the theoretical cross-section for each jet energy, assuming an LSP mass of 200 GeV, assuming a 100% BR of G→g+LSP and a small gluino lifetime (<3 hours).

12 Discussion

This is the first experimental study for this type of signal at a hadron collider. The results from 410 pb^{-1} of Tevatron data are already able to exclude a gluino mass in the range of 180-330 GeV, depending on the LSP mass, the theoretical conversion cross-section, and the gluino lifetime, assuming a 100% BR of G→g+LSP. The experience gained with the analysis methods and backgrounds involved allow us to have a good feel for the prospects of a stopped gluino search (or discovery!) in the future, both at the Tevatron with additional luminosity and at the nearly completed LHC, due to begin operation in 2007.

12.1 Extrapolation to Higher Integrated Luminosity

Assuming that no deviation is observed between the data and the expected background in the future, the 95% C.L. limits which could be set given additional luminosity should improve. One complication though is that the GAPSN triggers will become increasingly inefficient at higher instantaneous luminosities due to the increased probability of an overlapping min-bias interaction in an event during the gluino decay. However, since only the higher energy gluino decays will be of interest (because the lower energy decays have been excluded), the JT_125TT (or JT_95TT) trigger may be efficient by itself. There has also been effort to include a trigger during the "cosmic gaps" in the beam bunch structure, which would add an additional 20% trigger efficiency. Thus, it is safe to assume that overall trigger efficiency can remain at least as high as for this first analysis.

References

[1] N. Arkani-Hamed, S. Dimopoulos, G. F. Giudice and A. Romanino, Nucl. Phys. B **709**, 3 (2005) [arXiv:hep-ph/0409232].

[2] A. C. Kraan, Eur. Phys. J. C **37**, 91 (2004) [arXiv:hep-ex/0404001].

[3] A. Arvanitaki, S. Dimopoulos, A. Pierce, S. Rajendran and J. Wacker, arXiv:hep-ph/0506242.

[4] G. C. Blazey *et al.*, in *Proceedings of the Workshop: "QCD and Weak Boson Physics in Run II,"* edited by U. Baur, R. K. Ellis, and D. Zeppenfeld, (Fermilab, Batavia, IL, 2000) p. 47; see Sec. 3.5 for details.

13 Thanks

This work was motivated by the phenomenological studies of Jay Wacker, et al. from Stanford. He was also very helpful in discussing various theoretical issues related to this work. I also thank Dean Schamberger, Dan Edmunds, Gustaaf Brooijmans, John Parsons, and Terry Wyatt for their help, input, and support.